Local complete active space second-order perturbation theory using pair natural orbitals (PNO-CASPT2)

Filipe Menezes, Daniel Kats, Hans-Joachim Werner[a)1]

Institut für Theoretische Chemie, Universität Stuttgart, Pfaffenwaldring 55, D-70569 Stuttgart, Germany

We present a CASPT2 method which exploits local approximations to achieve linear scaling of the computational effort with the molecular size, provided the active space is small and local. The inactive orbitals are localized, and the virtual space for each electron pair is spanned by a domain of pair-natural orbitals (PNOs). The configuration space is internally contracted, and the PNOs are defined for uniquely defined orthogonal pairs. Distant pair energies are obtained by multipole approximations, so that the number of configurations that are explicitly treated in the CASPT2 scales linearly with molecular size (assuming a constant active space). The PNOs are generated using approximate amplitudes obtained in a pair-specific semi-canonical basis of projected atomic orbitals (PAOs). The evaluation and transformation of the two-electron integrals uses the same parallel local density fitting techniques as recently described for linear-scaling PNO-LMP2 (local second-order Møller-Plesset perturbation theory). The implementation of the amplitude equations, which are solved iteratively, employs the Local Integrated Tensor Framework (LITF). The efficiency and accuracy of the method is tested for excitation energies and correlation energies. It is demonstrated that the errors introduced by the local approximations are very small. They can be well controlled by few parameters for the distant pair approximation, initial PAO domains, and the PNO domains.

I. INTRODUCTION

Complete active space second-order perturbation theory[1–3] (CASPT2) is the simplest and probably most popular multi-reference electron correlation method. It has been widely used for computing excitation energies and electronic spectra, or to study molecules and reactions which cannot be treated by single-reference methods. Using multi-state extensions, it can also be applied to systems with near avoided crossings or conical intersections.[4–6] Analytical gradients are available for the single and multi-state versions,[6–8] which makes it possible to carry out geometry optimizations and to compute first-order molecular response properties for ground and excited states. The slow basis set convergence of the correlation energy has been much alleviated by explicitly correlated multi-reference (MR-F12) approaches,[5,9–12] and the integral evaluation speeded up using density fitting[8] (DF) or Cholesky decomposition[13] (CD) approaches. Thus, CASPT2 plays a similar role in the multi-reference regime as does second-order Møller-Plesset perturbation theory (MP2) in single-reference cases.

The standard CASPT2 method uses an effective Fock matrix in the zeroth-order Hamiltonian $\hat{H}^{(0)}$. Various choices of this operator have been proposed.[14–17] A drawback of constructing $\hat{H}^{(0)}$ solely using one-electron operators is the lack of exact size-consistency (but the errors are usually very small). This is related to the fact that in multi-reference cases the orbitals are not eigenfunctions of a single Fock operator, and therefore the CASSCF reference wavefunction is not an eigenfunction of $\hat{H}^{(0)}$, unless projection operators are introduced. Furthermore, CASPT2 sometimes suffers from so-called intruder state problems, which cause the wavefunction to blow up unless level shifts[18] are employed. These problems can be avoided using the N-electron valence state perturbation-theory (NEVPT2) approach.[19–24] The NEVPT2 method uses a similar wavefunction ansatz as CASPT2, but employs the Dyall zeroth-order Hamiltonian.[16] This also includes two-electron terms in $\hat{H}^{(0)}$, so that the CASSCF reference wavefunction is an eigenfunction of $\hat{H}^{(0)}$ without projection.

The accuracy of CASPT2 and NEVPT2 is often good, even though there are cases where perturbational approaches give qualitatively wrong results, see for example Ref. 25. According to our experience, the accuracy of CASPT2 and NEVPT2 is mostly comparable. Some improvements may be possible by using the third-order CASPT3[26] and NEVPT3[21] methods. For higher accuracy multireference configuration interaction (MRCI)[27–36] or multiconfiguration coupled-cluster (MRCC) methods[37–41] can be used, which are however computationally much more demanding. Perturbation and configuration interaction approaches can also be combined.[35]

As all conventional electron correlation methods, standard multi-reference approaches suffer from steep scaling of the computational cost with the molecular size. For a constant number of active orbitals, the cost of CASPT2 and MRCI scales as $\mathcal{O}(N^5)$ and $\mathcal{O}(N^6)$, respectively, where N is a measure of the molecular size. This is just as for MP2 or CCSD (coupled-cluster with single and double excitations), but with a higher prefactor (which depends on the active space). The polynomial scaling leads to a "scaling wall", which cannot be overcome. Even by using massively parallel computer hardware this wall can only be shifted to slightly larger molecular sizes. The

present paper is a contribution to solve this problem and to reduce the cost scaling of CASPT2 to linear by using local approximations. Much of the current work is based on previous advances for single reference methods, and these are therefore briefly summarized in the following.

Local correlation methods exploit the short-range character of electron correlation by using localized occupied molecular orbitals (LMOs).[42–92] In most of the older methods pair-specific domains of projected atomic orbitals[42] (PAOs) are used to describe the correlation of each electron pair. It turned out, however, that for each pair rather large domains (400-600 PAOs with triple-ζ basis sets) are necessary to robustly reach 99.8-99.9% of the canonical correlation energy and chemical accuracy (< 1 kcal mol^{-1}) for relative energies of large molecules. Despite linear scaling this may lead to enormous memory and disk space requirements. This problem was much alleviated by the pionering work of the Neese group,[83–91] who proposed to use pair-natural orbitals[29,93–96] in local coupled-cluster methods. This leads to a most compact representation of the wavefunction and fine-grained accuracy control. Since for the same accuracy the PNO domain sizes are typically an order of magnitude smaller than the PAO ones, the number of amplitudes is strongly reduced. The price to pay is that the virtual orbitals are different for each correlated orbital pair, leading to rather expensive integral transformations. This problem has been overcome by local density fitting approximations[57] and a combination of PAOs and PNOs.[88,91,92,97–100] Furthermore, basis set incompleteness errors as well as errors caused by the domain approximation can be much reduced by combining the local and explicitly correlated approaches.[97,99–106]

A conceptionally different approach is used in fragmentation[107–119] and incremental methods.[120–125] In these methods the correlation space is divided into subsystems, which are treated independently using conventional methods. The correlation energy is obtained as a linear combination of fragment energies. The regionally contracted MRCI of Hoyau et al.[126] also falls in this category, but here a final CI is carried out in the space of contracted incremental functions.

Much less work has been done to reduce the cost scaling for multireference methods. Carter and co-workers have developed local MRCI and MR-ACPF (multi-reference averaged coupled pair functional) methods.[79,127–129] They use a standard uncontracted MRCI ansatz,[27,28,130] localized orbitals in the reference function, and configuration selection using distance criteria. The virtual space is spanned by virtual localized orbitals (LVOs) or PAOs, and DF or CD approximations can be employed to evaluate the integrals.[129,131,132] An uncontracted local MRCC method has recently also been reported by Demel et al.[133]

A well known general problem with such uncontracted MRCI approaches is that the number of CSFs and the computational cost grow strongly with the number of reference configurations. This can be avoided by using internally contracted (IC) MR schemes, in which the configuration manifold is generated by applying excitation operators to the reference function as a whole. The IC wavefunction ansatz has been first proposed by Meyer[134] and somewhat later analyzed in more detail by Siegbahn.[135] To our knowledge, the first fully internally contracted MRCI implementation was reported by Werner and Reinsch.[136,137] Slightly later, internally contracted configurations (ICCs) were also used in the CASPT2 method of Roos et al.,[1] initially without semi-internal configurations. The great advantage of ICCs is that their number is similar as in single-reference cases and almost independent of the number of reference configurations. The difficulty, however, is that the structure of the ICCs is extremely complex. They are non-orthogonal and may even be linearly dependent. The overlap and Hamiltonian matrix elements depend on high-order reduced density matrices (RDMs) of the reference function; for fully contracted (FC) CASPT2 up to four particle RDMs (4-RDM) are needed, for MRCI even 5-RDMs. The orthogonalization requires the diagonalization of overlap matrices that depend on up to the 3-RDM and scales with M_{act}^9 (provided that in the MRCI case the uncontracted CAS space is used to relax the reference, since otherwise even the 4-RDM would be needed for the orthogonalization of the internal configurations and the 6-RDM for the Hamiltonian matrix elements). Another drawback of using ICCs is that the resulting wavefunctions are state-specific. ICCs are also used in the NEVPT2 method,[24] in the canonical transformation theory of Chan et al.[138–143], as well as in recent multireference coupled-cluster methods.[38–41]

In order to avoid the highest order RDMs in the overlap and Hamiltonian matrix elements, partially contracted MRCI and CASPT2 methods were developed[26,31–36] and since then used for uncountable applications. In the original partially contracted MRCI method of Werner and Knowles[26,31–34] only the doubly external configurations were contracted (now often denoted as WK contraction), and the inactive and active spaces (i.e., the "internal space") were treated on equal footing. This leads to a rather compact formulation involving only up to 4-RDMs of the internal space. Based on this ansatz, also multi-state versions of MRCI[34] and CASPT2[5,6] were proposed and implemented.

However, the computational cost of these methods rises quite steeply with the number of inactive orbitals. This problem was alleviated in CASPT2 and MRCI methods of Celani and Werner[35,144] and Shamasundar et al.,[36] in which the inactive orbital space is treated explicitly, and thus only active space RDMs are needed. Furthermore, also those singly external and internal configurations are contracted for which the overlap matrix can be expressed solely by the 1- and 2-RDMs of the active space (CW contraction). Unfortunately, the separation of the inactive and active spaces leads to very lengthy equations, in

particular for MRCI.[36] These equations were therefore derived using computer algebra programs and stored in a human-readable algorithm file as a long sequence of binary tensor contractions. The algorithm file can be executed efficiently using the integrated tensor framework (ITF) originally developed by Knizia,[36,145] and for some cases this even outperforms well optimized hand-coded programs. More recently, the ITF has been generalized to treat local approximations by one of us.[65,66] Further extensions for using PNOs have been made in the course of the current work, cf. section III D.

In the current paper we describe a local PNO-CASPT2 method, which reduces the scaling of the computational cost to linear in the number of inactive orbitals (for a fixed active space). The inactive orbital space is localized, and the PNOs are generated using approximate amplitudes obtained in large PAO-domains. Our formulation is invariant to unitary transformations within the active space. Even though the active space can often be well localized, this cannot be fully exploited since the orthogonalization of the ICCs effectively mixes contributions of all active orbitals. For some subspaces, the orthogonalization is equivalent to a transformation to natural active orbitals (which diagonalize the 1-RDM in the active space). On the other hand, the equations and approximations for double excitations from the inactive orbital space are very similar as in single-reference closed-shell MP2. In fact, in the absence of active orbitals our PNO-CASPT2 method reduces to the PNO-LMP2 method recently described.[99]

Very recently, Guo et al.[146] have reported a NEVPT2 method, which uses "domain-based local PNOs" (DLPNOs) to reduce the computational effort and scaling for large molecules. "Domain-based" means that the PNOs are generated using domains of PAOs, just as in the PNO-CASPT2 method described in the current paper (but for simplicity we omit the prefix "DL'). Guo et al. also implemented the so-called "strongly contracted" variant of NEVPT2,[20] but due to lack of orbital invariance this proved to be less useful for local approximations. The developments of the DLPNO-NEVPT2 and our PNO-CASPT2 methods were completely independent and without knowing of each other, but many of the conclusions turned out to be similar. Although the DLPNO-NEVPT2 and our PNO-CASPT2 are based on the same fully contracted wavefunction ansatz (both state-specific and without relaxation of the reference function), they differ in the choice of the zeroth-order Hamiltonian and various other details. Both methods achieve near linear scaling of the computational cost with molecular size, provided the active space is constant and local. For example, this should be very useful for treating transition metal complexes with large ligands, where the active space only involves the transition metal(s) and possibly a small region in its vicinity. But even for cases where the active space is not local, the PNO treatment may save considerable CPU time.

Our paper is organized as follows: in section II we will first outline the general CASPT2 theory and then introduce the local approximations. In section III we will describe some details of our implementation. Benchmarks to demonstrate the scaling, computational efficiency, and accuracy of the method will be presented in section IV. Finally, a summary and conclusions will be given.

II. THEORY

As usual, the orbital space will be divided into core (not correlated), inactive (closed-shell), active, and virtual (external) subsets. For the sake of simplicity, we will not explicitly distinguish between core and inactive orbitals, but in our computer program this is of course done. Unless otherwise noted, inactive orbitals will be denoted with indices i, j, k, l, active orbitals with indices t, u, v, w, x, y, z, and virtual orbitals by indices a, b. Indices m, n will run over the inactive and active spaces (also denoted the "internal" space).

A. The wavefunction ansatz and zeroth-order Hamiltonian

The reference (zeroth-order) wavefunction is of complete active space [CAS(N, M)] type, i.e. it includes all configuration state functions (CSFs) of a given symmetry and spin which can be formed by distributing N electrons in M active orbitals,

$$|\Psi_0^{(n)}\rangle = \sum_R |\Phi_R\rangle c_R^{(n)}. \quad (1)$$

The orbitals are usually optimized in a CASSCF (complete active space self-consistent field) calculation, which can be either state-specific or state averaged. Often it is also helpful to take the inactive orbitals (or a subspace of those) from a preceding Hartree-Fock calculation and freeze them in the CASSCF. This strongly reduces the computational effort for the CASSCF without much affecting the results (cf. section IV).

The superscript (n) denotes the state to be optimized. At the current stage, our PNO-CASPT2 method is state-specific, and we will therefore omit the state label in the following and use the simplified notation $|0\rangle \equiv |\Psi_0^{(n)}\rangle$. A well known disadvantage of single-state CASPT2 calculations is that the reference coefficients c_R are fixed and not relaxed. This restriction can be (partly) lifted by multi-state (MS) CASPT2 treatments,[4–6] which may be important in near degeneracy situations, as for instance in the vicinity of conical intersections. An extension of the PNO-CASPT2 theory to such MS cases should in principle be possible, but this has not been derived and implemented so far.

We assume intermediate normalization, $\langle 0|0\rangle = 1$ and use a fully spin-adapted formulation, employing the spin-summed excitation operators

$$\hat{E}^r_i \equiv \hat{E}_{ri} = \hat{a}^\dagger_{r\alpha}\hat{a}_{i\alpha} + \hat{a}^\dagger_{r\beta}\hat{a}_{i\beta}, \tag{2}$$

$$\hat{E}^{rs}_{ij} \equiv \hat{E}_{ri,sj} = \hat{E}_{ri}\hat{E}_{sj} - \delta_{is}\hat{E}_{rj}, \tag{3}$$

$$\hat{E}^{qrs}_{ijk} \equiv \hat{E}_{qi,rj,sk} = \hat{E}_{qi,rj}\hat{E}_{sk} - \delta_{is}\hat{E}_{qk,rj} - \delta_{js}\hat{E}_{qi,rk}, \tag{4}$$

where i, j, k are any occupied and q, r, s any active or virtual orbitals. For convenience in later expressions, we define n-particle active space density reduced matrices (n-RDMs)

$$D^{(1)}_{tu} = \langle 0|\hat{E}_{tu}|0\rangle, \tag{5}$$

$$D^{(2)}_{tu,vw} = \langle 0|\hat{E}_{tu,vw}|0\rangle, \tag{6}$$

$$D^{(3)}_{tu,vw,xy} = \langle 0|\hat{E}_{tu,vw,xy}|0\rangle, \tag{7}$$

and so on. Furthermore, we also define hole-particle excitation operators

$$\check{E}_{tu} = \hat{a}_{t\alpha}\hat{a}^\dagger_{u\alpha} + \hat{a}_{t\beta}\hat{a}^\dagger_{u\beta} \tag{8}$$

and the corresponding active-space hole-particle density matrices

$$\bar{D}_{tu} = 2\delta_{tu} - D^{(1)}_{ut}, \tag{9}$$

$$\begin{aligned}\bar{D}_{tu,vw} = {} & 4\delta_{ut}\delta_{wv} - 2\delta_{wt}\delta_{uv} \\ & -2\delta_{ut}D^{(1)}_{wv} - 2\delta_{wv}D^{(1)}_{ut} \\ & +\delta_{uv}D^{(1)}_{wt} + \delta_{wt}D^{(1)}_{uv} + D^{(2)}_{wv,ut}.\end{aligned} \tag{10}$$

The reference energy can be written in terms of the active space density matrices as

$$E_0 = \sum_{tu} f^c_{tu}D^{(1)}_{tu} + \frac{1}{2}\sum_{tu,vw}(tu|vw)D^{(2)}_{tu,vw} + E_c + E_{\text{nuc}}. \tag{11}$$

Here f^c_{rs} is the closed-shell Fock matrix (r, s any orbitals),

$$f^c_{rs} = \langle r|\hat{h}|s\rangle + \sum_j^{\text{closed}}\big[2(rs|jj) - (rj|js)\big], \tag{12}$$

E_{nuc} the nuclear repulsion energy, and E_c the closed-shell energy $E_c = \sum_i^{\text{closed}}(h_{ii} + f^c_{ii})$.

The first-order wavefunction is expanded in a configuration basis $\{\Phi_\lambda\}$ that is orthogonal to the reference function $|0\rangle$, i.e. it does not include any of the reference configurations $|\Phi_R\rangle$,

$$\Psi^{(1)} = \sum_\lambda |\Phi_\lambda\rangle T_\lambda, \qquad \langle\Phi_\lambda|0\rangle = 0\,. \tag{13}$$

The specific internally contracted configurations $|\Phi_\lambda\rangle$ used in this work will be defined in section II B. The amplitudes T_λ are optimized by minimizing the Hylleraas functional

$$E_2 = 2\langle\Psi^{(1)}|\hat{H}|0\rangle + \langle\Psi^{(1)}|\hat{H}^{(0)} - E^{(0)}|\Psi^{(1)}\rangle. \tag{14}$$

The minimum of this functional corresponds to the second-order correlation energy $E^{(2)}$. In CASPT2 the zeroth-order Hamiltonian $\hat{H}^{(0)}$ is usually defined as[1–3]

$$\hat{H}^{(0)} = \hat{P}\hat{F}\hat{P} + \hat{Q}\hat{F}\hat{Q}, \tag{15}$$

$$E^{(0)} = \langle 0|\hat{F}|0\rangle, \tag{16}$$

where $\hat{P} = |0\rangle\langle 0|$ and $\hat{Q} = 1 - \hat{P}$ project onto the reference function and its orthogonal complement, respectively. The projection operators are necessary since (in contrast to the single reference case) the reference function $|0\rangle$ is not an eigenfunction of the Fock operator $\hat{F}$, which in the current work is taken as

$$\hat{F} = \sum_{rs}\hat{E}_{rs}f_{rs}, \tag{17}$$

$$f_{rs} = f^c_{rs} + \sum_{tu}D^{(1)}_{tu}\big[(rs|tu) - \frac{1}{2}(ru|ts)\big]. \tag{18}$$

For clarity of the equations we will sometimes use the tensor notation $f^s_r = f_{rs}$. Modified definitions of the operator $\hat{F}$ have also been proposed in the past.[14–17] In contrast to NEVPT2, the CASPT2 zeroth-order Hamiltonian does not explicitly include contributions of the all-active two-electron integrals $(tu|vw)$, but it does include all couplings $H^{(0)}_{\lambda\lambda'} = \langle\Phi_\lambda|\hat{F}|\Phi'_\lambda\rangle$. In NEVPT2, which used the Dyall Hamiltonian[16], additional projectors are introduced, which make the matrix representation of $H^{(0)}$ block-diagonal in different configuration subspaces.

Minimization of the Hylleraas functional leads to the first-order amplitude equations

$$R_\lambda = \langle\tilde{\Phi}_\lambda|\hat{H}|0\rangle + \langle\tilde{\Phi}_\lambda|\hat{H}^{(0)} - \hat{E}^{(0)}|\Psi^{(1)}\rangle = 0 \;\;\forall\,\lambda. \tag{19}$$

Using the notation $K_\lambda = \langle\tilde{\Phi}_\lambda|\hat{H}|0\rangle$ the Hylleraas functional can be rewritten more compactly as

$$E_2 = \sum_\lambda \tilde{T}_\lambda(K_\lambda + R_\lambda). \tag{20}$$

where $\langle\tilde{\Phi}_\lambda|$ are suitable contravariant configurations which are defined such that $\langle\tilde{\Phi}_\lambda|\Phi_{\lambda'}\rangle = \delta_{\lambda\lambda'}$, and therefore

$$\langle\tilde{\Phi}_\lambda|\Psi^{(1)}\rangle = T_\lambda. \tag{21}$$

The corresponding amplitudes $\tilde{T}_\lambda$ are defined such that

$$\Psi^{(1)} = \sum_\lambda |\tilde{\Phi}_\lambda\rangle\tilde{T}_\lambda = \sum_\lambda |\Phi_\lambda\rangle T_\lambda. \tag{22}$$

B. Definition of the internally contracted configuration space

Internally contracted configurations (ICCs) are obtained by applying the excitation operators to the reference function as a whole, e.g.

$$|\Phi^{rs}_{mn}\rangle = \hat{E}^{rs}_{mn}|0\rangle = \sum_R c_R \hat{E}^{rs}_{mn}|\Phi_R\rangle, \qquad (23)$$

where m, n run over all correlated orbitals (inactive and active) and r, s over all active and virtual orbitals. This includes all excitation operators in the Hamiltonian which give non-zero contributions if $\hat{H}$ is applied to the reference, and therefore a linear independent subset of the $|\Phi^{rs}_{mn}\rangle$ exactly spans the first-order interacting space.[134] The configuration set $|\Phi^{rs}_{mn}\rangle$ implicitly also includes single excitations. The first-order wavefunction can then be expressed as

$$|\Psi^{(1)}\rangle = \frac{1}{2}\sum_{mn}\sum_{rs}|\Phi^{rs}_{mn}\rangle T^{mn}_{rs}. \qquad (24)$$

In practice one may also use suitable linear combinations of the ICCs, as will be discussed further below.

In order to orthogonalize the ICCs we first classify them according to the number of electrons in the virtual orbitals, and the number of holes in the inactive space. As in our earlier work on IC-CASPT2[144] and IC-MRCI[35,36] we denote configurations with 0, 1, or 2 electrons in virtual orbitals by indices I (internals), S (singles and semi-internals), and P (pairs), respectively. Furthermore, we add a subscript to these letters which corresponds to the number of holes in the inactive space. This leads to 8 configuration classes $P_2, P_1, P_0, S_2, S_1, S_0, I_2, I_1$. The I_0 space is included in the reference space and does therefore not belong to the excitation space. All the 8 subspaces are mutually orthogonal. Furthermore, configurations with different holes in the inactive space are orthogonal. The overlap matrices and thus the transformations to the orthogonal configurations within each subspace only depend on density matrices of the active space and are independent of the inactive and virtual orbital labels.

The definition of the non-orthogonal ICCs for the 8 subspaces is summarized in Table I. Instead of using the configurations defined in eq. (23) directly, we found it convenient to use singlet ($p = 1$) and triplet ($p = -1$) configurations for the P_0 and I_2 spaces. The singlet and triplet configurations are mutually orthogonal. Note that for P_0 $|\Phi^{ab}_{tu,p}\rangle = p|\Phi^{ba}_{tu,p}\rangle$, but for computational convenience we include all indices a, b in the summations. A similar symmetry holds for the I_2 configurations. For the P_2, P_1, and S_2 spaces we use the listed contravariant configurations, for the other spaces the co- and contravariant functions are identical.

We note that single excitations $|\Phi^a_i\rangle = \hat{E}^a_i|0\rangle$ are redundant with the semi-internal configurations $|\Phi^{ta}_{ti}\rangle$ in the S_1 space, and need only be included if no active orbitals are present (but then the method reduces to closed-shell MP2 and single excitations are not needed if the Brillouin condition is fulfilled). In the following formalism, we will omit the single excitations, even though they can optionally be included in our program.

TABLE I. Definition of unique non-orthogonal ICCs for the 8 subspaces. The configurations Φ^{rs}_{mn} are defined in eq. (23).

Space	configuration	Index restrictions
P_0:	$\|\Phi^{ab}_{tu,p}\rangle = \frac{1}{2}\big[\|\Phi^{ab}_{tu}\rangle + p\|\Phi^{ab}_{ut}\rangle\big]$,	$t \geq u,\ a \geq b,\ p = \pm 1$
P_1:	$\|\Phi^{ab}_{ti}\rangle$	
P_2:	$\|\Phi^{ab}_{ij}\rangle$	$i \geq j$
S_0:	$\|\Phi^{av}_{tu}\rangle$	
S_1:	$\|\Phi^{av}_{ti}\rangle$, $\|\Phi^{va}_{ti}\rangle$	
S_2:	$\|\Phi^{av}_{ij}\rangle$	
I_1:	$\|\Phi^{vw}_{ti}\rangle$	
I_2:	$\|\Phi^{vw}_{ijp}\rangle = \frac{1}{2}\big[\|\Phi^{vw}_{ij}\rangle + p\|\Phi^{vw}_{ji}\rangle\big]$,	$i \geq j,\ v \geq w,\ p = \pm 1$
Contravariant configurations:		
P_1:	$\langle\tilde{\Phi}^{ab}_{it}\| = \frac{1}{3}\big[2\langle\Phi^{ab}_{it}\| + \langle\Phi^{ba}_{it}\|\big]$	
P_2:	$\langle\tilde{\Phi}^{ab}_{ij}\| = \frac{1}{6}\big[2\langle\Phi^{ab}_{ij}\| + \langle\Phi^{ba}_{ij}\|\big]$	$i \geq j$
S_2:	$\langle\tilde{\Phi}^{av}_{ij}\| = \frac{1}{3}\big[2\langle\Phi^{av}_{ij}\| + \langle\Phi^{av}_{ji}\|\big]$	

In terms of these configurations the elements of the overlap matrices $\mathbf{S}$ for the 8 subspaces are summarized in Table II. In order to orthogonalize the configurations, one has to find for each individual subspace a transformation $\mathbf{X}$, such that

$$\mathbf{X}^\dagger \mathbf{S} \mathbf{X} = \mathbf{1}. \qquad (25)$$

We use $X_{\mu\lambda} = \bar{X}_{\mu\lambda} s_\lambda^{-\frac{1}{2}}$, where $\bar{X}_{\mu\lambda}$ are the eigenvectors of $\mathbf{S}$ with eigenvalues s_λ and the index μ refers to the non-orthogonal configurations. If the eigenvalues s_λ are below a certain threshold (default 10^{-7}), the corresponding eigenvectors are removed and $\mathbf{X}$ becomes a rectangular matrix. In the active-space overlap matrix elements such as e.g. $S^{P_0,p}_{tu,vw}$ the superscript refers to the space, and the subscripts left and right of the comma are considered as compound row and column indices of the corresponding overlap matrix [restrictions such as $t \geq u$, $v \geq w$ may apply as shown in Table I; note that for the triplet ($p = -1$) configurations the diagonal elements $t = u$ and $a = b$ give no contribution, but for simplicity this is not explicitly shown in the Tables]. The corresponding transformation matrix elements are written as e.g. $X^{P0,p}_{tu} \equiv X^{(p)}_{tu,P_0}$. Here we use the space symbols such as P_0 also as running index for the different eigenvectors and orthogonal configurations (index λ above).

The orthogonal ICCs defined in this way are not unique, since each subspace can be further transformed by any unitary transformation. Unique configurations can be defined by block-diagonalizing the zeroth order Hamiltonian in each subspace. For example, for the P_0 and P_1

TABLE II. Overlap matrices and orthogonal ICCs for the 8 subspaces. In the last column, summations over repeated indices are implied, using the same index restriction as in Table I.

Space	overlap	active space overlap matrix	orthogonal ICCs
P_0:	$\langle\Phi^{ab}_{tu,p}\vert\Phi^{cd}_{vw,q}\rangle = \frac{1}{2}\delta_{pq}(\delta_{ac}\delta_{bd} + p\delta_{ad}\delta_{bc})S^{P_0,p}_{tu,vw}$	$S^{P_0,p}_{tu,vw} = D^{(2)}_{tv,uw} + pD^{(2)}_{tw,uv}$	$\vert\Phi^{ab}_{P_0,p}\rangle = \vert\Phi^{ab,p}_{tu}\rangle V^{P_0,p}_{tu}$
P_1:	$\langle\tilde{\Phi}^{ab}_{ti}\vert\Phi^{cd}_{uj}\rangle = \delta_{ij}\delta_{ac}\delta_{bd}S^{P_1}_{t,u}$	$S^{P_1}_{t,u} = D^{(1)}_{tu}$	$\vert\Phi^{ab}_{P_1,i}\rangle = \vert\Phi^{ab}_{ti}\rangle V^{P_1}_{t}$
P_2:	$\langle\tilde{\Phi}^{ab}_{ij}\vert\Phi^{cd}_{kl}\rangle = \delta_{ik}\delta_{jl}\delta_{ac}\delta_{bd} + \delta_{ik}\delta_{jl}\delta_{ad}$		
S_0:	$\langle\Phi^{ax}_{tu}\vert\Phi^{by}_{vw}\rangle = \delta_{ab}S^{S_0}_{tux,vwy}$	$S^{S_0}_{tux,vwy} = D^{(3)}_{tv,ux,yw} - \delta_{xy}D^{(2)}_{tv,uw}$	$\vert\Phi^{a}_{S_0}\rangle = \vert\Phi^{ax}_{tu}\rangle V^{S_0}_{tux}$
S_1:	$\langle\Phi^{xa}_{ti}\vert\Phi^{yb}_{uj}\rangle = 2\delta_{ab}\delta_{ij}S^{S_1}_{tx,uy}$	$S^{S_1}_{tx,uy} = \delta_{xy}D^{(1)}_{tu} + D^{(2)}_{tx,yu}$	
	$\langle\Phi^{ax}_{ti}\vert\Phi^{yb}_{uj}\rangle = -\delta_{ab}\delta_{ij}S^{S_1}_{tx,uy}$		$\vert\Phi^{a}_{S_1,i}\rangle = \vert\Phi^{xa}_{ti}\rangle V^{S_1}_{tx} + \vert\Phi^{ax}_{ti}\rangle \tilde{V}^{S_1}_{tx}$
	$\langle\Phi^{ax}_{ti}\vert\Phi^{by}_{uj}\rangle = \frac{1}{2}\delta_{ab}\delta_{ij}\bar{S}^{S_1}_{tx,uy}$	$\bar{S}^{S_1}_{tx,uy} = 2\delta_{xy}D^{(1)}_{tu} - D^{(2)}_{tu,yx}$	
S_2:	$\langle\tilde{\Phi}^{ax}_{ij}\vert\Phi^{by}_{kl}\rangle = \delta_{ab}\delta_{ik}\delta_{jl}S^{S_2}_{x,y}$	$S^{S_2}_{x,y} = \bar{D}^{(1)}_{yx}$	$\vert\Phi^{a,S_2}_{ij}\rangle = \vert\Phi^{ax}_{ij}\rangle V^{S_2}_{x}$
I_1:	$\langle\Phi^{vw}_{ti}\vert\Phi^{xy}_{uj}\rangle = \delta_{ij}S^{I_1}_{vwt,xyu}$	$S^{I_1}_{tvw,uxy} = D^{(1)}_{tu}(2\delta_{vx}\delta_{wy} - \delta_{wx}\delta_{vy})$	
		$-\delta_{vy}D^{(2)}_{tw,xu} - \delta_{wx}D^{(2)}_{tv,yu} - \delta_{vx}D^{(2)}_{tu,yw}$	$\vert\Phi^{I_1}_{i}\rangle = \vert\Phi^{vw}_{ti}\rangle V^{I_1}_{vwt}$
		$+2\delta_{wy}D^{(2)}_{tv,xu} - D^{(3)}_{tv,xu,yw}$	
I_2:	$\langle\Phi^{tu}_{ij,p}\vert\Phi^{vw}_{kl,q}\rangle = \frac{1}{2}\delta_{pq}(\delta_{ik}\delta_{jl} + p\delta_{il}\delta_{jk})S^{I_2,p}_{tu,vw}$	$S^{I_2,p}_{tu,vw} = \bar{D}^{(2)}_{tv,uw} + p\bar{D}^{(2)}_{tw,uv}$	$\vert\Phi^{I_2}_{ij,p}\rangle = \vert\Phi^{tu}_{ij,p}\rangle V^{I_2,p}_{tu}$

subspaces the matrices to be diagonalized are

$$C^{(p)}_{P_0,P_0'} = \delta_{pq}\sum_{t\geq u}X^{P_0,p}_{tu}\sum_{v\geq w}X^{P_0',q}_{vw} \sum_{xy}(D^{(3)}_{tv,uw,xy} + pD^{(3)}_{tw,uv,xy})f_{xy}, \quad (26)$$

$$C_{P_1,P_1'} = \sum_{t}X^{P_1}_{t}\sum_{u}X^{P_1'}_{u}\sum_{vw}D^{(2)}_{tu,vw}f_{vw}. \quad (27)$$

Diagonalizing the $C^{(p)}_{P_0,P_0'}$-matrix yields a unitary transformation $\mathbf{U}^{(P_0,p)}$ The total transformation matrix is then

$$V^{P_0,p}_{tu} = \sum_{P_0'}X^{P_0',p}_{tu}U^{P_0,p}_{P_0'}, \quad (28)$$

and the final orthogonal P_0 configurations are defined as

$$\vert\Phi^{ab}_{P_0,p}\rangle = \sum_{t\geq u}\vert\Phi^{ab}_{tu,p}\rangle V^{P_0,p}_{tu}. \quad (29)$$

Similar transformations of the active space indices are possible for each other subspace. Note that for the S_1 space there are two kinds of configurations, $\vert\Phi^{xa}_{ti}\rangle$ and $\vert\Phi^{ax}_{ti}\rangle$, which are not mutually orthogonal. Therefore, compound overlap and $\mathbf{C}$ matrices of the form

$$\begin{pmatrix} 2\mathbf{S}^{S_1} & -\mathbf{S}^{S_1} \\ -\mathbf{S}^{S_1} & \bar{\mathbf{S}}^{S_1} \end{pmatrix}, \quad \begin{pmatrix} 2\mathbf{C}^{S_1} & -\mathbf{C}^{S_1} \\ -\mathbf{C}^{S_1} & \bar{\mathbf{C}}^{S_1} \end{pmatrix} \quad (30)$$

have to be used for the orthogonalization, where the blocks with the overbar refers to the configurations $\vert\Phi^{ax}_{ti}\rangle$. Correspondingly, the transformation matrices are written as

$$\begin{pmatrix} \mathbf{X}^{S_1} \\ \bar{\mathbf{X}}^{S_1} \end{pmatrix}, \quad \begin{pmatrix} \mathbf{V}^{S_1} \\ \bar{\mathbf{V}}^{S_1} \end{pmatrix}. \quad (31)$$

The above procedure defines a unique set of orthogonal configurations and at the same time minimizes the couplings via the zeroth-order Hamiltonian. The energy of a conventional CASPT2 is invariant to the transformation $\mathbf{U}$, and the only effect of this transformation is a simplification of the amplitude equations and an optimally fast convergence when solving the amplitude equations iteratively. However, when making local approximations, it is essential to have a unique definition of the orthogonal pairs, since the correlation subspace for each pair is different. This will be further discussed in section II D.

It should be noted that due to the different zeroth-order Hamiltonian the definition of the orthogonal configurations is different in the DLPNO-NEVPT2 method of Guo et al.[146] Furthermore, due to the use of the Dyall Hamiltonian there are no couplings between the 8 configuration subspaces in the NEVPT2 method.

In the orthogonalized configuration space, we define the first-order wavefunction as

$$\Psi^{(1)} = \sum_{a,b}\left[\sum_{P_0}\sum_{p=\pm1}|\Phi^{ab}_{P_0,p}\rangle T^{P_0,p}_{ab} + \sum_{P_1,i}|\Phi^{ab}_{i,P_1}\rangle T^{P_1,i}_{ab} + \frac{1}{2}\sum_{i,j}|\Phi^{ab}_{ij}\rangle T^{ij}_{ab}\right] + \sum_{a}\left[\sum_{S_0}|\Phi^{a}_{S_0}\rangle t^{S_0}_{a} + \sum_{S_1}\sum_{i}|\Phi^{a}_{i,S_1}\rangle t^{S_1,i}_{a} + \sum_{S_2}\sum_{i,j}|\Phi^{a,S_2}_{ij}\rangle t^{ij}_{a,S_2}\right] + \sum_{I_1}\sum_{i}|\Phi^{I_1}_{i}\rangle t^{i}_{I_1} + \sum_{I_2}\sum_{i\geq j}\sum_{p=\pm1}|\Phi^{I_2}_{ij,p}\rangle t^{ij,p}_{I_2}. \tag{32}$$

Here we write amplitude matrices such as T^{ij}_{ab} in upper case; the superscripts denote different matrices and the subscripts the matrix elements. Amplitude vectors such as $t^{S_0}_a$ are written in lower case.

C. Amplitude equations

In a conventional CASPT2 implementation it is possible to compute the residuals in the non-orthogonal configuration basis, and transform them to the orthogonal basis just for the amplitude update. This transformation is necessary to remove linear dependencies and to ensure fast convergence. The amplitude updates $\Delta\mathbf{t}$ are subsequently back-transformed to the non-orthogonal basis, for example for S_0:

$$R^{S_0}_a = \sum_{tuv} V^{S_0}_{tuv} R^{tuv}_a, \tag{33}$$

$$\Delta t^{S0}_a = -\frac{R^{S_0}_a}{\epsilon^{S_0}_a}, \tag{34}$$

$$\Delta t^{tuv}_a = \sum_{S_0} V^{S_0}_{tuv}\Delta t^{S_0}_a. \tag{35}$$

The update Δt^{tuv}_a is then added to the previous coefficients t^{tuv}_a. The advantage of this procedure is that all integrals and density matrices that are needed to compute the residuals R^{tuv}_a are directly related to orbital labels and independent of the transformation matrices $\mathbf{V}$. However, in our local treatment this is not possible for the P_0 and P_1 spaces, since PNO domains will be defined for each orthogonal pair (cf. section II D). The transformations would then mix different PNO domains. Therefore, we need to express the residuals $R^{P_0}_{ab}$ and $P^{P_1}_{ab}$, as well as all contributions of the amplitudes $T^{P_0}_{ab}$ and $T^{P_1}_{ab}$ to these and other residuals in the orthogonal ICC basis. As will be discussed in section II D, we use PAO domains for the S_0 and S_1 spaces, and these domains are independent of the active labels. Therefore, for these spaces (as well as for the I_1 and I_2 spaces) one can either compute the residuals in the orthogonal or in the non-orthogonal ICC basis. Which way is more efficient depends on the numbers of active and virtual orbitals. Computing the residuals in the orthogonal basis has the advantage that due to redundancies the number of residuals may be significantly smaller than in the non-orthogonal basis, and the amplitudes must not be back transformed to the non-orthogonal basis. However, the transformations have to be applied to many intermediate quantities, and for the S_0 and I_1 spaces some of these transformations scale as M^9_{act}, where M_{act} is the number of active orbitals. If the transformation is done as shown in eq. (33), it scales only as $M^6_{\mathrm{act}}M_{\mathrm{virt}}$ (for S_0). The best choice may therefore depend on the ratio of virtual to active orbitals. For consistency, we will present all equations in the orthogonal basis, but it is straightforward to reorder the summations to obtain the form in eq. (33). In our program the residuals for the I_1 and S_0 spaces are evaluated in the non-orthogonal basis, in order to avoid the M^9_{act} transformation mentioned above.

In order to illustrate the structure of the equations, we will only present the residual for the P spaces here, since these will be relevant in section II D for the PNO generation. All other residuals can be found in the supporting information. We assume that the virtual block of the Fock matrix is diagonal with eigenvalues ϵ_a, and that the matrices $C^{(p)}_{P_0,P_0'}$ [cf. eq. (26)] and $C_{P_1,P_1'}$ [cf. eq. (27)] are diagonal with eigenvalues $c^{P_0,p}$, c^{P_1}, respectively. Since the zeroth-order Hamiltonian only contains one-electron operators, the P spaces can only couple with the S spaces. Straightforward algebra yields for the matrix elements $\langle\tilde{\Phi}_\lambda|\hat{H}|0\rangle$, which are needed to compute the correlation energy,

$$\langle\tilde{\Phi}^{ab}_{ij}|\hat{H}|0\rangle = K^{ij}_{ab}, \tag{36}$$

$$\langle\tilde{\Phi}^{ab}_{P_1,j}|\hat{H}|0\rangle = \sum_t \left[\mathbf{V}^{P_1\,\dagger}\mathbf{S}^{P_1}\right]^{P_1}_{t} K^{tj}_{ab} \equiv K^{P_1,j}_{ab}, \tag{37}$$

$$\langle\Phi^{ab}_{P_0,p}|\hat{H}|0\rangle = \sum_{t\geq u}\frac{1}{1+\delta_{tu}}\left[\mathbf{V}^{P_0,p\,\dagger}\mathbf{S}^{P_0,p}\right]^{P_0,p}_{tu} K^{tu,p}_{ab} \equiv K^{P_0,p}_{ab}, \tag{38}$$

where $K^{mn}_{ab} = (a\,m|b\,n)$ are the two-electron repulsion integrals in Mulliken notation, and

$$K^{tu,p}_{ab} = \frac{1}{2}\left(K^{tu}_{ab} + pK^{tu}_{ba}\right). \tag{39}$$

The residuals for the three pair classes can be written as

$$R_{ab}^{ij} = K_{ab}^{ij} + \epsilon_{ab}^{ij} T_{ab}^{ij} + G_{ab}^{ij} + G_{ba}^{ji}, \quad (40)$$
$$R_{ab}^{P_1,j} = K_{ab}^{P_1,j} + \epsilon_{ab}^{P_1,j} T_{ab}^{P_1,j} + G_{ab}^{P_1,j}, \quad (41)$$
$$R_{ab}^{P_0,p} = K_{ab}^{P_0,p} + \epsilon_{ab}^{P_0,p} T_{ab}^{P_0,p} + G_{ab}^{P_0,p} + pG_{ba}^{P_0,p}. \quad (42)$$

Within each space and for given inactive orbitals i, j the zeroth-order Hamiltonian is diagonal, and the diagonal matrix elements of $\hat{H}^{(0)} - E^{(0)}$ are

$$\epsilon_{ab}^{ij} = \epsilon_a + \epsilon_b - f_{ii} - f_{jj}, \quad (43)$$
$$\epsilon_{ab}^{P_1,j} = \epsilon_a + \epsilon_b + c^{P_1} - f_{jj} - E_{\rm act}^{(0)}, \quad (44)$$
$$\epsilon_{ab}^{P_0,p} = \epsilon_a + \epsilon_b + c^{P_0,p} - E_{act}^{(0)}, \quad (45)$$

where $E_{act}^{(0)} = \sum_{tu} D_{tu}^{(1)} f_{tu}$. The couplings between different configuration blocks are described by the matrices

$$G_{ab}^{ij} = -\sum_{k\neq j} T_{ab}^{ik} f_k^j - \frac{1}{2}\sum_{P_1} f_{P_1}^i T_{ab}^{P_1,j} + \frac{1}{2}\sum_{S_2} t_a^{ij,S_2} f_b^{S_2} + f_a^i \sum_{S_1} t_b^{S_1,j}\sigma_{S_1}, \quad (46)$$

$$G_{ab}^{P_1,j} = -\sum_{k\neq j} T_{ab}^{P_1,k} f_k^j - \sum_p \frac{1}{(2-p)} \sum_{P_0} f_{P_0,p}^{P_1,j} T_{ab}^{P_0,p} - \sum_k f_k^{P_1} T_{ab}^{kj} + f_a^j \sum_{S_0} t_b^{S_0}\sigma_{S_0}^{P_1} + \sum_{S_1} (f_{a,S_1}^{P_1} t_b^{S_1,j} + t_a^{S_1,j} \bar{f}_{S_1,b}^{P_1}), \quad (47)$$

$$G_{ab}^{P_0,p} = -\sum_{P_1,j} f_{P_1,j}^{P_0,p} T_{ab}^{P_1,j} + \sum_{S_0} f_{a,S_0}^{P_0,p} t_b^{S_0}. \quad (48)$$

The coupling coefficients are contractions of transformed density matrices with Fock-matrix elements :

$$f_{P_1,i}^{P_0,p} = \frac{1}{2}\sum_t f_{it} \sum_u V_u^{P_1} \sum_{vw} S_{tu,vw}^{P_0,p} V_{vw}^{P_0,p}, \quad (49)$$
$$f_{a,S_0}^{P_0,p} = \sum_x f_{ax} \sum_{tu} V_{tu}^{P_0,p} \sum_{vwy} S_{tux,vwy}^{S_0} V_{vwy}^{S_0}, \quad (50)$$
$$f_{a,S_1}^{P_1} = \sum_v f_{av} \sum_t V_t^{P_1} \sum_{uw} (S_{tv,uw}^{S_1} V_{uw}^{S_1} - \tilde{S}_{tw,vu} \bar{V}_{uw}^{S_1}), \quad (51)$$
$$\bar{f}_{S_1,b}^{P_1} = \sum_v f_{bv} \sum_t V_t^{P_1} \sum_{uw} (D_{tu}^{(1)}\delta_{vw} - \tilde{S}_{tw,uv}) \bar{V}_{uw}^{S_1}, \quad (52)$$
$$f_i^{P_1} = \sum_t f_{it} \sum_u D_{tu}^{(1)} V_u^{P_1}, \quad (53)$$
$$f_b^{S_2} = \sum_{tu} V_u^{S_2} S_{ut}^{S_2} f_{tb}, \quad (54)$$
$$\sigma_{S_1} = \sum_{tu} D_{tu}^{(1)} (V_{tu}^{S_1} - \frac{1}{2}\bar{V}_{tu}^{S_1}), \quad (55)$$
$$\sigma_{S_0}^{P_1} = \sum_t V_t^{P_1} \sum_{uvw} D_{ut,wv}^{(2)} V_{vwu}^{S_0}, \quad (56)$$

where

$$\tilde{S}_{tu,vw} = \frac{1}{3}(2D_{tv,uw}^{(2)} + D_{tw,uv}^{(2)}). \quad (57)$$

We have also used $f_i^{P_1} = f_{P_1}^i$ and $f_{P_0,p}^{P_1,j} = f_{P_1,j}^{P_0,p}$. The residuals have been implemented using a local version[65,66] of the integrated tensor framework (ITF).[36,145] More details will be given in section III D.

D. Definition of PNOs and domains

In order to achieve linear scaling of the computation time and required memory with the molecular size local approximations are introduced. These approximations are very similar as for single reference cases: the occupied orbitals are localized, and the excitations for each pair are restricted to pair-specific domains of local virtual orbitals. Furthermore, the small energy contributions of distant pairs (i.e. those where the orbitals i and j are spatially far apart) can be neglected or approximated by a multipole treatment (cf. section II E).

In the current work we use a two-step procedure to define the domains: first, large pair domains of projected atomic orbitals (PAOs) are generated. PAOs are defined as[42]

$$|\phi_{\tilde{r}}^{\rm PAO}\rangle = \Big(1 - \sum_m |m\rangle\langle m|\Big)|\phi_{\tilde{r}}^{\rm AO}\rangle, \quad (58)$$

where $|\phi_{\tilde{r}}^{\rm AO}\rangle$ are suitable atomic orbitals (normally basis functions). In the following, the non-orthogonal PAOs will be labeled by indices $\tilde{r}, \tilde{s}$. The PAO domains are used to obtain a non-iterative approximation for the pair amplitudes. Secondly, pair natural orbitals (PNOs) are constructed from these amplitudes. This leads to a strong reduction of the domain sizes. The intermediate use of PAO domains is necessary in order to avoid an $\mathcal{O}(N^5)$ [or $\mathcal{O}(N^4)$ if distant pairs are excluded] scaling of the PNO generation step. This is very similar as in previous work on PNO-LMP2[99,100] and PNO-LCCSD.[88,92,97]

However, in the multireference case there are some additional subtleties to consider. As already pointed out in section II B, a unique set of orthogonal pair functions must be constructed, in order to obtain a unique set of PNOs and well defined energies. Furthermore, one has to define suitable domains for the semi-internal configurations (S_0, S_1, and S_2) spaces. For the S_2 space one can use the domains of the corresponding P_2 pairs, since both spaces describe the correlation of a unique ij pair, and the corresponding PNOs are independent of the transformation $\mathbf{V}^{S_2}$. However, for the P_0 and P_1 spaces the PNOs depend on the $\mathbf{V}^{P_0,p}$ and $\mathbf{V}^{P_1}$ transformations, which are different than the transformations for the S_0 and S_1 spaces. Thus, there is no direct relation between the (P_1, i) and (S_1, i) spaces, and the number of

P_1 and S_1 functions is different. The same holds for the S_0 and P_0 spaces. One possibility that we tested is to use the PNO domains of the diagonal pairs (ii) for the semi-internal configurations (S_1, i). However, it turned out that these PNOs are not well suited, and the loss in correlation energy is significant. This was also found in the recent local PNO-NEVPT2 method by Guo et al.;[146] these authors used enlarged PNO domains of the (ii) pairs, obtained with a very small PNO occupation number threshold. We found it simpler and more accurate not to use PNOs for the S_1 and S_0 spaces at all. Instead, we use PAO domains. The construction of these domains will be described further below.

The orbitals are localized separately for the inactive and active orbitals. As in our other recent local methods, we use in the current work intrinsic bond orbitals (IBOs).[147] This type of localization yields LMOs and partial atomic charges that are very insensitive to the basis set. The partial charges can therefore be conveniently used to define orbital domains. Since our formulation is invariant to unitary transformations among the active orbitals, the localization of the active orbitals does not affect the results. We therefore localize the active orbitals only in order to define the PAO domains in a unique way, as described below. However, in the actual calculation the natural or canonical active orbitals that result from the preceding CASSCF calculation are used, since then also the reference vector $\mathbf{c}$ can be directly taken from the CASSCF. Note that with natural active orbitals the P_1 and S_2 spaces are automatically orthogonal, since the corresponding overlap matrices only depend on the 1-RDM.

In our implementation the PAO domains are center based, i.e. all PAOs that arise from the AOs at selected centers are included in the domain. Thus, all domains are uniquely defined by center lists. The selection of the centers for the orbital domains proceeds in two steps: As in our previous work on PNO-LMP2, *primary* orbital domains are selected based on the partial IBO charges, and by default include all centers with charges $\geq T_{\mathrm{LMO}}$ (default $T_{\mathrm{LMO}} = 0.2$). Secondly, extended domains are created by adding neighboring centers to the primary domain for each LMO. Neighboring atoms are those which are connected to any atom within the primary domain by up to `IEXT` bonds, or within a radius of `REXT` bohr. For simplicity, we use by default `REXT=2*IEXT+1` bohr. The connectivity criterion `IEXT` has the advantage that it is independent of the bond lengths (two atoms are considered to be bonded if their distance is smaller than 1.2 times the sum of the atomic radii). On the other hand, the distance criterion also covers the case that two non-bonded atoms happen to be close (e.g. at transition states or in molecular clusters). In many cases `IEXT=1` is sufficient, but for high accuracy `IEXT=2` (default) is recommended. Examples will be given in section IV C.

The PAO orbital domains for the inactive orbitals are denoted $[i]_{\mathrm{PAO}}$. A special treatment is necessary for the active space. Since it is not possible to assign specific active orbitals to the configuration classes S_1, S_0, P_1, and P_0, we use the union of the domains $[t]_{\mathrm{PAO}}$ of all active orbitals t to define a single active domain $[act]_{\mathrm{PAO}}$. This domain is assigned to all active orbitals.

Next, pair domains $[ij]_{\mathrm{PAO}} = [i]_{\mathrm{PAO}} \cup [j]_{\mathrm{PAO}}$ (used for S_2 and P_2 pairs) and $[act, j]_{\mathrm{PAO}} = [act]_{\mathrm{PAO}} \cup [j]_{\mathrm{PAO}}$ for the (S_1, j) and (P_1, j) configuration spaces are created. The P_0 and S_0 spaces solely use the $[act]_{\mathrm{PAO}}$ domain. Each pair domain generated in this way is orthogonalized and made pseudo-canonical (PC) by diagonalizing the Fock matrix in the subspace of the domain. This is exactly as in the PNO-LMP2 case and we refer to previous work[99] for further details. The orthogonal PC-PAOs will be denoted by indices r, s, and the corresponding orbital energies are denoted ϵ_r^{ij}, $\epsilon_r^{P_1,j}$, and $\epsilon_r^{P_0}$. The resulting PC-PAOs are different for each pair, and strictly they should therefore be labeled by indices r^{ij}, $r^{P_1,j}$, r^{P_0}. For the sake of simplicity, we will in the following omit the superscripts on the PAO labels r, s since they always belong to the same pair domain as indicated by the superscripts of the amplitude or integral matrices to which they belong. The transformations from the non-orthogonal PAO domains to the orthonormal PC-PAO domains are described by matrices $[\mathbf{W}^{ij}_{\mathrm{PAO}}]_{\tilde{r}r}$.

Once the PC-PAO domains are known, the integrals K^{ij}_{rs}, $K^{P_1,j}_{rs}$, and $K^{P_0}_{rs}$ are computed. More details about this step will be given in section III B. By neglecting the matrices $\mathbf{G}$ in eqs. (46)–(48) we can then obtain a semi-canonical (SC) approximation for the pair amplitudes

$$T^{ij}_{rs} = -K^{ij}_{rs}/\epsilon^{ij}_{rs}, \qquad \tilde{T}^{ij}_{rs} = 2T^{ij}_{rs} - T^{ij}_{sr} \tag{59}$$

$$T^{P_1,j}_{rs} = -K^{P_1,j}_{rs}/\epsilon^{P_1,j}_{rs}, \quad \tilde{T}^{P_1,j}_{rs} = 2T^{P_1,j}_{rs} - T^{P_1,j}_{sr} \tag{60}$$

$$T^{P_0,p}_{rs} = -K^{P_0,p}_{rs}/\epsilon^{P_0,p}_{rs}, \tag{61}$$

where the denominators are given by eqs. (43)–(45) with a, b replaced by the PC-PAO labels r, s. Using these amplitudes, external pair densities

$$D^{ij}_{rs} = \frac{1}{1+\delta_{ij}} \left[\tilde{\mathbf{T}}^{ij\dagger}\mathbf{T}^{ij} + \tilde{\mathbf{T}}^{ij}\mathbf{T}^{ij\dagger}\right]_{rs}, \tag{62}$$

$$D^{P_1,j}_{rs} = \left[\tilde{\mathbf{T}}^{P_1,j\dagger}\mathbf{T}^{P_1,j} + \tilde{\mathbf{T}}^{P_1,j}\mathbf{T}^{P_1,j\dagger}\right]_{rs}, \tag{63}$$

$$D^{P_0,p}_{rs} = \left[\mathbf{T}^{P_0,p\dagger}\mathbf{T}^{P_0,p}\right]_{rs} \tag{64}$$

are computed and diagonalized, which yields the unitary transformations from the PC-PAO to the PNO basis, e.g. for the P_2 space:

$$\left[\mathbf{W}^{ij\dagger}_{\mathrm{PNO}}\mathbf{D}^{ij}\mathbf{W}^{ij}_{\mathrm{PNO}}\right]_{\bar{a}\bar{b}} = n^{ij}_{\bar{a}}\delta_{\bar{a}\bar{b}}. \tag{65}$$

Again, we use the simplified notation that the PNO indices $\bar{a}, \bar{b}$ refer to the PNOs for the pair, which is indicated by the superscripts of the corresponding matrix.

The PNO domains (i.e. the columns of the matrices $\mathbf{W}_{\mathrm{PNO}}$ that are kept) are selected by two criteria: the

first is based on the natural occupation numbers $n_{\bar{a}}^{ij}$, and all PNOs for which $n_{\bar{a}}^{ij} \geq T_{\mathrm{PNO}}^{\mathrm{occ}}$ are included. In our program the default value for the threshold is $T_{\mathrm{PNO}}^{\mathrm{occ}} = 10^{-8}$.

The occupation number criterion works well for spatially close orbital pairs, but may lead to too small or even empty domains for more distant orbital pairs. This may lead to a significant underestimation of long-range dispersion energies.[99] In order to avoid this problem, an additional completeness criterion based on the pair energies must be satisfied. The semi-canonical PAO pair energies are

$$E_{ij}^{\mathrm{PAO}} = (2 - \delta_{ij}) \sum_{rs \in [ij]_{\mathrm{PAO}}} \tilde{T}_{rs}^{ij} K_{rs}^{ij}, \quad (i \geq j) \tag{66}$$

$$E_{P1,j}^{\mathrm{PAO}} = 2 \sum_{rs \in [P_1,j]_{\mathrm{PAO}}} \tilde{T}_{rs}^{P_1,j} K_{rs}^{P_1,j}, \tag{67}$$

$$E_{P0,p}^{\mathrm{PAO}} = \sum_{rs \in [P_0]_{\mathrm{PAO}}} T_{rs}^{P_0,p} K_{rs}^{P_0,p}. \tag{68}$$

The integral matrices and amplitude matrices are transformed to the PNO basis, e.g. $\mathbf{K}_{\bar{a}\bar{b}}^{ij} = \left[\mathbf{W}_{\mathrm{PNO}}^{ij\dagger} \mathbf{K}^{ij} \mathbf{W}_{\mathrm{PNO}}^{ij}\right]_{\bar{a}\bar{b}}$, $\mathbf{T}_{\bar{a}\bar{b}}^{ij} = \left[\mathbf{W}_{\mathrm{PNO}}^{ij\dagger} \mathbf{T}^{ij} \mathbf{W}_{\mathrm{PNO}}^{ij}\right]_{\bar{a}\bar{b}}$, and then corresponding PNO pair energies are computed using these matrices but with reduced PNO domains $\bar{a}, \bar{b} \in [ij]_{\mathrm{PNO}}$. Initially, the domains selected by the occupation-number criterion are used. Then further PNOs (in the order of decreasing natural occupation numbers) are added until the criterion

$$\frac{E_{ij}^{\mathrm{PNO}}}{E_{ij}^{\mathrm{PAO}}} \geq T_{\mathrm{PNO}}^{\mathrm{en}} \tag{69}$$

is satisfied. The default value is $T_{\mathrm{PNO}}^{\mathrm{en}} = 0.997$. The transformations and domain selections for the P_1 and P_0 spaces are completely analogous.

Again, the block of the Fock matrix in the PNO domain $F_{\bar{a}\bar{b}}^{ij} = \sum_{r \in [ij]_{\mathrm{PAO}}} W_{r\bar{a}}^{ij} \epsilon_r^{ij} W_{r\bar{b}}^{ij}$ ($\bar{a}, \bar{b} \in [ij]_{\mathrm{PNO}}$) is diagonalized to get pseudo-canonical PNOs (labeled a, b) with orbital energies ϵ_a^{ij}. The integral matrices are transformed accordingly. In the following it will always be assumed that the virtual orbitals are pseudo-canonical and that $[\mathbf{W}_{\mathrm{PNO}}^{ij}]_{ra}$ includes the latter transformation. Finally, total transformation matrices from the non-orthogonal PAO basis to the pseudo-canonical PNO basis

$$[\mathbf{W}^{ij}]_{\tilde{r}a} = [\mathbf{W}_{\mathrm{PAO}}^{ij} \cdot \mathbf{W}_{\mathrm{PNO}}^{ij}]_{\tilde{r}a} \tag{70}$$

are formed and stored. These matrices (and similar ones for the P_1 and P_2 pairs) are needed to compute the overlap matrices between different PNO domains, see below.

In summary, we have now pseudo-canonical pair domains $[ij]_{\text{PC-PNO}}$ for the P_2 and S_2 spaces, $[P_1, j]_{\text{PC-PNO}}$ for the P_1 space, $[P_0, p]_{\text{PC-PNO}}$ for the P_0 space, $[act, j]_{\text{PC-PAO}}$ for the S_1 space, and $[act]_{\text{PC-PAO}}$ for the S_0 space. For each of these a matrix $\mathbf{W}$ exists, which transforms from the non-orthogonal PAO basis to the corresponding pseudo-canonical pair basis. Note that for the S_1 and S_0 spaces the transformations are independent of the running labels S_1 and S_0. The S_1 and S_0 residuals are calculated in the non-orthogonal PAO basis, and only transformed to the pseudo-canonical basis for the update procedure. This strongly reduces the number of transformation and overlap matrices to be stored. Additionally, the system-inherent domains[148] can be employed for the S_1 and S_0 spaces in order to reduce the memory demand and computational cost; however, this was not utilized in the current implementation. For simplicity, we will in the following drop the subscripts PC-PNO or PC-PAO for the domain specifications, i.e. $[ij] \equiv [ij]_{\text{PC-PNO}}$ and $[act, j] \equiv [act, j]_{\text{PC-PAO}}$.

Due to the fact that the PNOs for different pairs are mutually non-orthogonal, the amplitudes that occur in the $\mathbf{G}$ matrices must be multiplied with overlap matrices between the domains that are involved in the interaction. For example, the first and last terms in $\mathbf{G}^{ij}$ [eq. (46)] become in the PNO basis:

$$\begin{aligned} G_{[ij],[ij]} &= -\sum_{k \neq j} \mathbf{S}_{[ij],[ik]} \mathbf{T}_{[ik],[ik]}^{ik} \mathbf{S}_{[ik],[ij]} f_k^j + \ldots \\ &\quad + f_{[ij]}^i \left[\mathbf{S}_{[ij],[act,j]} \sum_{S_1} \mathbf{t}_{[act,j]}^{S_1,j} \sigma_{S_1}\right]^\dagger \end{aligned} \tag{71}$$

where

$$\mathbf{S}_{[ij],[ik]} = \left[\mathbf{W}^{ij\,\dagger} \mathbf{S}_{\mathrm{PAO}} \mathbf{W}^{ik}\right]_{[ij],[ik]}, \tag{72}$$

$$\mathbf{S}_{[ij],[act,j]} = \left[\mathbf{W}^{ij\,\dagger} \mathbf{S}_{\mathrm{PAO}} \mathbf{W}_{\mathrm{PAO}}^{act,j}\right]_{[ij],[act,j]}, \tag{73}$$

and $[\mathbf{S}_{\mathrm{PAO}}]_{\tilde{r}\tilde{s}} = \langle \tilde{r} | \tilde{s} \rangle$ is the overlap matrix of the PAOs. The subscripts in square brackets indicate the domains of the corresponding matrix or vector indices; e.g., $\mathbf{S}_{[ij],[ik]}$ is the overlap matrix between the PC-PNO domains $[ij]$ and $[ik]$, while $\mathbf{S}_{[ij],[act,j]}$ is the overlap matrix between the PC-PNO-domain $[ij]$ and the PC-PAO domain $[act, j]$. Similar transformations with overlap matrices occur in all other terms of the $\mathbf{G}$ matrices.

We finally note that the domain selection procedure in the DLPNO-NEVPT2 program of Guo et al.[146] is slightly different. They choose PAO domains based on a differential overlap integral criterion, cf. eq. (23) of their paper. Furthermore, in the PNO domain selection they do not employ the additional completeness criterion [eq. (69)], and do not use different PNOs for singlet and triplet pairs for the P_0 space. Due to the different definitions of the NEVPT2 and CASPT2 $\hat{H}^{(0)}$ operators, the unique P_0 and P_1 pairs (obtained by block-diagonalizing $\hat{H}^{(0)}$) are not the same in both approaches, which could also affect the PNO domain approximation. The effect of these differences on domain sizes and results would require a detailed comparison of both methods, which has not been possible so far. Most likely, the effect is small.

E. Distant pair approximations

Without further approximations, the number of pairs and amplitudes still scales quadratically with the molecular size (for a constant number of active orbitals). In order to achieve linear scaling, the two-electron integrals such as $(ri|sj)$ for distant pairs ij can be approximated by multipole expansions. The values of these integrals decay exponentially with the distances between the local orbitals r and i or s and j. Therefore, if i and j are spatially far apart, the integrals have only sizable values if r is close to i and s close to j. Thus, it is assumed that $r^i \in [ii]_{\text{PC-PAO}}$ and $s^j \in [jj]_{\text{PC-PAO}}$, and exchange-type integrals $(s^j i|r^i j)$ as well as charge-transfer terms $(r^i i|s^i j)$ are neglected. The multipole approximation is based on the fact that the densities ρ_{ri}, ρ_{sj} carry no charge, i.e. $\int \rho_{ri}(r)dr = 0$. Then the first contribution in the long-range multipole expansion is the dipole-dipole interaction of the charge densities $\rho_{ri}(r_1)$ and $\rho_{sj}(r_2)$, and the simplest approximation for the integrals is[88]

$$(r^i i|s^j j) \approx \frac{\sqrt{2}}{R_{ij}^3}\big[\langle r^i|\hat{x}|i\rangle\langle s^j|\hat{x}|j\rangle + \langle r^i|\hat{y}|i\rangle\langle s^j|\hat{y}|j\rangle + \langle r^i|\hat{z}|i\rangle\langle s^j|\hat{z}|j\rangle\big], \quad (74)$$

where R_{ij} is the distance between the charge centers of i and j. Using these integrals, the distant pair energies E_{ij} can be approximated using eqs. (59) and (66). This is exactly as in the closed-shell case. More accurate higher order multipole approximations are also possible and have been used in the past.[49,50] In the current work we employ only the simple form of eq. (74). Based on this approximation, all pairs (ij) are fully included in the PNO-CASPT2 for which $E_{ij} \geq T_{\text{dist}}$ (the default is $T_{\text{dist}} = 10^{-6}\ E_h$).

Integrals such as $(ai|tj)$ or $(ui|tj)$ decay exponentially with the distance between the inactive and active orbitals, and therefore these contributions could be entirely neglected if $R_{j,t} > R_{\text{dist}}$. The distance between two orbitals is defined as the shortest distance between any atoms in the primary domains. In order to keep the invariance with respect to unitary transformations in the active space, the shortest distance $R_{j,act} = \min(\{R_{jt}\}$ for any active orbital t is used, and the integrals and corresponding pairs are neglected if $R_{j,act} > R_{\text{dist}}$, where R_{dist} is a distance criterion. Such criteria are applied to the P_1, S_1, S_2, I_1, and I_2 spaces, with a default value of $R_{\text{dist}} = 15$ bohr. In addition, the S_2 and I_2 spaces are restricted to the P_2 pair list. Using the default value of R_{dist}, the error caused by the distance criterion for the $[(C_4SH_3)\text{-}[CH_2]_{50}\text{-}(C_4SH_3)]^{2+}$ system (see section IV) amounts only to 10 μH.

Currently, the multipole approximation is only applied for the P_2 space. We note, however, that multipole approximations would also be possible for other spaces. If natural orbitals are used for the active space, the configurations $|\Phi_{tj}^{ab}\rangle$ (P_1 space) are automatically orthogonal and the natural orbital label t corresponds to the label P_1 (since $V_t^{P_1} = \delta_{P_1,t}$). The integrals $(ta|jb)$ can then be approximated as above and the energy contribution E_{ti} be computed on the fly without storing the integrals. Similarly, with natural active orbitals the S_2 space is orthogonal, i.e., $|\Phi_{ij}^{rt}\rangle = |\Phi_{ij}^{r,S_2}\rangle$, and the integrals $(ia|jt)$ could also be approximated by a multipole expansion.

For the remaining spaces the multipole approximation is more complicated, since the energy contributions cannot be computed without transforming the integrals to the orthogonal ICC basis. Naturally, distant pair approximations should not be needed for the P_0 and S_0 spaces, since we assume that the active space is local. Furthermore, for the S_1 and I_1 spaces the matrix elements $\langle\Phi_\lambda|\hat{H}|0\rangle$ also depend on Fock matrix elements, which may give long-range contributions. One must also be careful to avoid multipole approximations for integrals such as $(ri|tt)$. In this case the dipole-dipole approximation is not valid, since the charge distributions ρ_{tt} carry a charge of 1. A detailed analysis shows, however, that all such integrals can be replaced by Fock matrix elements.

Multipole approximations for these spaces as well as higher-order multipole approximations will be investigated in future work and reported elsewhere.

III. IMPLEMENTATION

In this section we summarize some details about the implementation of our PNO-CASPT2 method.

A. Computation of density matrices

For the fully contracted CASPT2 method one needs the active space density matrices up to third order as well as a contraction of the 4-RDM with the Fock matrix elements f_{tu} (see below). The 3-RDM is computed by using eq. (4) and the resolution of the identity in the CAS space $\sum_I |I\rangle\langle I|$ as

$$D^{(3)}_{tu,vw,xy} = \sum_I \langle 0|\hat{E}_{tu,vw}|I\rangle\langle I|\hat{E}_{xy}|0\rangle - \delta_{wx}D^{(2)}_{tu,vy} - \delta_{ux}D^{(2)}_{ty,vw} \quad (75)$$

The transition densities $A_{I,xy} = \langle I|\hat{E}_{xy}|0\rangle$ are precomputed and kept in memory. The two-particle transition densities $B^{(tv)}_{uw,I} = \langle 0|\hat{E}_{tu,vw}|I\rangle$ are computed on-the-fly for fixed indices $t \geq v$. These quantities are evaluated using a spin-adapted CSF basis and the efficient symmetric group technique described in Ref. 32. The 1-RDM and 2-RDM are then obtained as matrix-vector products, and the contribution to the 3-RDM by a matrix multiplica-

tion:

$$D^{(1)}_{xy} = \left[\mathbf{A}^\dagger \mathbf{c}\right]_{xy} \quad (76)$$

$$D^{(2)}_{tu,vw} = \left[\mathbf{B}^{(tv)} \mathbf{c}\right]_{uw} \quad (77)$$

$$\sum_I \langle 0|\hat{E}_{tu,vw}|I\rangle \sum_J \langle I|\hat{E}_{xy}|0\rangle = [\mathbf{B}^{(tv)}\mathbf{A}]_{uw,xy}, \quad (78)$$

where uw and xy are composite indices, and $\mathbf{c}$ is the reference coefficient vector. The algorithm requires that the 2-RDM and 3-RDM as well as the matrix $\mathbf{A}$ and one matrix $\mathbf{B}^{(tv)}$ fit into memory. If the memory is insufficient, it would be possible to page over blocks of intermediate CSFs I, but this was not necessary for any calculation in this paper. Parallelization is over the indices tu.

In addition, one needs in CASPT2 the contractions

$$E^{(0)}_{act} = \sum_{tu} D^{(1)}_{tu} f_{tu}, \quad (79)$$

$$D^{2f}_{tu} = \sum_{vw} D^{(2)}_{tu,vw} f_{vw}, \quad (80)$$

$$D^{3f}_{tu,vw} = \sum_{xy} D^{(3)}_{tu,vw,xy} f_{xy}, \quad (81)$$

$$D^{4f}_{tu,vw,xy} = \sum_{zz'} D^{(4)}_{tu,vw,xy,zz'} f_{zz'}. \quad (82)$$

The evaluation of the first three quantities is of course trivial once the density matrices (up to the 3-RDM) are available. The contraction of the 4-RDM can be written as

$$D^{4f}_{tu,vw,xy} = \sum_I \langle 0|\hat{E}_{tu,vw,xy}|0^f\rangle - \sum_z D^{(3)}_{tu,vw,xz} f_{yz} - \sum_z D^{(3)}_{tu,vz,xy} f_{wz} - \sum_z D^{(3)}_{tz,vw,xy} f_{uz}, \quad (83)$$

where

$$|0^f\rangle = \sum_I |I\rangle d^f_I, \qquad d^f_I = \sum_{zz'} \langle I|\hat{E}_{zz'}|0\rangle f_{zz'}. \quad (84)$$

The first term of eq. (83) can be computed in exactly the same way as eq. (75) by using in all ket functions the vector $\mathbf{d}^f$ rather than the reference vector $\mathbf{c}$. In this way the additional effort for computing the contribution of the 4-RDM is even less than the effort for computing the 3-RDM, since the intermediates $\mathbf{B}^{(tv)}$ can be used for both. Apart from the lower-order terms, only the modified matrix $[\mathbf{A}^f]_{I,xy} = \langle I|\hat{E}_{xy}|0^f\rangle$ needs to be precomputed and stored, and an additional matrix multiplication as in eq. (78) is required.

The calculation of all density matrices and contractions D^{nf} ($n \leq 4$) takes about 1 and 40 sec for CAS(10,10) (19404 CSFs) and CAS(12,12) (226512 CSFs) reference functions, respectively (using 4 compute cores). Due to the factorial scaling of the number of reference configurations with the number of active orbitals the computational effort grows steeply for larger active spaces.

B. Linear-scaling integral evaluation

For the CASPT2 method one first needs the integrals $K^{mn}_{\tilde{r}\tilde{s}}$ (2-external), $K^{mn}_{\tilde{r}t}$, $K^{nm}_{\tilde{r}t} = K^{mn}_{t\tilde{r}}$ (1-external), and K^{mn}_{tu} (0-external), where the labels $m \geq n$ run over all correlated LMOs, t, u over the active space, and $\tilde{r}, \tilde{s}$ over the non-orthogonal PAOs of the domain $[mn]_{\mathrm{PAO}}$. In order to avoid separate integral evaluations for the three integral classes, we extend in the integral transformation each PAO domain $[mn]_{\mathrm{PAO}}$ by the active orbitals, so that each matrix $\mathbf{K}^{mn}$ then consists of the blocks

$$\mathbf{K}^{mn} \equiv \begin{pmatrix} K^{mn}_{\tilde{r}\tilde{s}} & K^{mn}_{\tilde{r}u} \\ K^{mn}_{t\tilde{s}} & K^{mn}_{tu} \end{pmatrix}, \qquad \tilde{r}, \tilde{s} \in [mn]_{\mathrm{PAO}} \quad (85)$$

These integral matrices are computed using local density fitting (LDF)[57] with the same parallel program as described recently for PNO-LMP2.[99,100] If sparsity of the LMO and PAO matrices is used as described in detail in Ref. 99, the transformation scales linearly (provided the active space is local). Here we use the same default truncation thresholds as in Ref. 100, i.e. $T_{\mathrm{LMO}} = T_{\mathrm{PAO}} = 10^{-6}$.

Subsequently, for each matrix $\mathbf{K}^{mn}$ the 4 blocks are separated, and the 2-external blocks $K^{mn}_{\tilde{r}\tilde{s}}$ are transformed to the PC-PAO basis using the transformation matrices $\mathbf{W}^{mn}_{\mathrm{PAO}}$. The 1-external blocks are stored as vectors, e.g., $K^{txj}_r \equiv K^{tj}_{xr}$, $\bar{K}^{txj}_r \equiv K^{tj}_{rx}$ (S_1), and $K^{tux}_r \equiv K^{tu}_{rx}$ (S_0). These integrals are left in the non-orthogonal PAO basis since the transformation to the PC-PAO basis is more conveniently done at a later stage. The all-internal integrals are stored as K^{ij}_{vw} (I_2), and $K^{i}_{vwt} \equiv K^{ti}_{vw}$ (I_1). The all-active integrals K^{tu}_{vw} are only needed for computing the reference energy. In our program the reference energy and the reference CI-vector $\mathbf{c}$ can be taken directly from the preceding MCSCF calculation, and in this case these integrals are not needed and not stored.

The final step is to transform the integrals for the various spaces to the orthogonal ICC basis, as shown in eqs. (37) and (38) for the P_1 and P_0 spaces, respectively. For the other spaces the transformations are (cf. Table II)

$$K^{S_0}_r = \sum_{tvw} \left[\mathbf{V}^{S_0\,\dagger}\, \mathbf{S}^{S_0}\right]^{S_0}_{tvw} K^{tvw}_r, \quad (86)$$

$$K^{S_1,j}_r = \sum_{tv} \left[(2\mathbf{V}^{S_1} - \tilde{\mathbf{V}}^{S_1})^\dagger\, \mathbf{S}^{S_1}\right]^{S_1}_{tv} K^{tvj}_r + \sum_{tv} \left[\tilde{\mathbf{V}}^{S_1\dagger}\, \tilde{\mathbf{S}}^{S_1} - \mathbf{V}^{S_1\,\dagger} \mathbf{S}^{S_1}\right]^{S_1}_{tv} \tilde{K}^{tvj}_r, \quad (87)$$

$$K^{S_2,ij}_r = \sum_{t} \left[\mathbf{V}^{S_2\,\dagger}\, \mathbf{S}^{S_2}\right]^{S_2}_{t} K^{tij}_r, \quad (88)$$

$$K^{i}_{I_1} = \sum_{tuv} [\mathbf{V}^{I_1\,\dagger}\, \mathbf{S}^{I_1}]^{I_1}_{tuv} K^{i}_{tuv}, \quad (89)$$

$$K^{ij}_{I_2,p} = \sum_{t\geq u} \frac{1}{1+\delta_{tu}} \left[\mathbf{V}^{I_2,p\,\dagger}\, \mathbf{S}^{I_2,p}\right]^{I_2}_{tu} K^{ij,p}_{tu}. \quad (90)$$

The integrals $K_{tu}^{ij,p}$ are defined as in eq. (39). Note that for the S_1, S_0, and I_1 spaces also Fock matrix elements contribute to the corresponding terms $\langle\Phi_\lambda|\hat{H}|0\rangle$, which are not included above.

C. Parallelization

The integral transformation and PNO generation is fully parallelized using the Global Array (GA) software.[149] (see http://hpc.pnl.gov/globalarrays). The integral transformation uses a dynamical parallelization model, as described in Refs. 99 and 100. Subsequently, the pairs are distributed over processors. In order to be able to carry out the transformations of the integrals from the non-orthogonal to the orthogonal ICC basis (cf. section III B) in parallel and without communication, it is necessary to store all integrals for the P_0 and S_0 spaces on the same processor. Similarly, for the P_1, S_1, and I_1 spaces all integrals for the same closed-shell orbital j must be stored on the same processor, and so the distribution is over the index j. Finally, the P_2, S_2, and I_2 pairs are distributed so that the total number of pairs on each processor is as similar as possible. The transformations and the PNO generation can then be done independently for the pairs on the individual processors and scales well over multiple compute nodes. However, since the ITF implementation described in section III D is at the current stage only moderately parallel, the overall parallel speedup is only modest, and the program only works on shared file systems (i.e., within one compute node). A fully scalable multi-node implementation will be developed in future.

D. Local ITF implementation of the amplitude equations

The PNO-CASPT2 amplitude equations have been implemented using the local integrated tensor framework (LITF).[65,66] For this the framework has been extended to handle the transformations of active-space quantities such as density matrices to the orthogonalized ICC spaces, to define the PNO spaces, as well as to introduce non-triangular pair lists, which are used to define the PNO domains in the P_1 space. Additionally, tensor contractions have been parallelized over loops using a shared file approach.

For quantities in the PNO basis one often needs indices to address particular PNO domains or domain blocks. Each PNO domain is associated to a (orthogonal) pair number or two orbital numbers. These indices are not present in the tensor itself, they just are used for addressing specific tensors or tensor blocks. They are therefore denoted *phantom tensor indices*. For example, the PNO overlap matrices $S_{[ij],[ik]}$ in Eq. (71) require 4 additional *phantom* occupied indices to define each domain block; these correspond to the indices in square brackets.

Such phantom tensor indices have been introduced already before for tensors in the OSV basis.[65] They are even more essential for an efficient PNO implementation, since united domains cannot be used in the PNO case. This kind of indices has some unique properties in the contractions, i.e., the summations usually do not run over these indices.

It has been shown before[65,66] that the LITF algorithms are quite efficient for solving residual equations, but are less efficient for calculating integrals. Therefore the integrals as well as the density matrices and PNOs are calculated using native programming-language routines as described in section III. Then the integrals, density matrices, orthogonalization tensors and PAO to PNO transformation matrices are imported into the LITF, and everything else is calculated therein.

IV. BENCHMARKS

The procedures described in section III have been implemented into the development version of `MOLPRO`.[145,150] In addition, a new non-local fully contracted CASPT2 program has been implemented, in order to compare directly results with and without local approximations. Both programs include the usual level shift procedure with energy correction,[18] and unless otherwise noted a shift of 0.3 E_h has been used in all CASPT2 calculations.

A. Computational details

In most calculations the aug-cc-pVDZ orbital basis[151,152] was used; for a subset of molecules also the corresponding triple-ζ and quadruple$-\zeta$ basis sets have been employed. For second-row atoms such as S or P the aug-cc-pV(X+d)Z sets[153] were used. For simplicity, these basis sets will in the following be denoted AVDZ, AVTZ, etc. It is normally sufficient to omit the diffuse functions on hydrogen atoms, and such mixed basis sets are denoted AVDZ', AVTZ', etc. The CASSCF calculations were carried out with the density fitting implementation[8] in `MOLPRO`, using the corresponding JKFIT auxiliary basis sets of Weigend.[154] Unless otherwise noted, the original non-augmented sets were employed, but in some cases we also used the augmented JKFIT sets that are available in `MOLPRO` (these were obtained from the standard sets by adding one diffuse function for each angular momentum in an even-tempered manner). The effect of the additional diffuse functions in the JKFIT basis was found to be very small ($\leq$ 0.001 eV for excitation energies). The effective Fock matrix [eq. (18)] used in the zeroth-order Hamiltonian has been computed in the MCSCF program

using the JKFIT auxiliary basis. Also the reference energy and the reference coefficients are directly taken from the MCSCF. The calculation of these quantities is not included in the timings given later in this section. All two-electron integrals that were used in the PNO-CASPT2 method were computed using local density fitting as described in section III B using the MP2FIT auxiliary basis sets[155] which correspond to the orbital basis. In all CASPT2 calculations only the valence orbitals were correlated.

B. Optimization of the reference functions

A major problem for CASPT2 calculations on large molecules is the choice of the active spaces and the MCSCF optimization of the reference function. For the molecules studied in this work the choices of the active space was quite straightforward. In most cases it comprises all π-orbitals of the aromatic systems; in some cases also interacting lone pairs from neighboring oxygen or nitrogen atoms were included. The character of the active space orbitals has been carefully checked, since (depending on the starting guess) it can easily happen that the MCSCF procedure converges to an undesired solution. Unless otherwise noted, the lowest two singlet states have been included in the state-averaged MCSCF (SA-MCSCF) optimization. We are employing the second-order optimization MCSCF method described in Refs. 156 and 157, which normally converges very fast and robustly. However, such second-order methods become very expensive for large molecules, since all integrals with up to two virtual orbitals are needed. In order to avoid excessive MCSCF optimization times, we used for some of the larger molecules frozen inactive orbitals. It turned out that often canonical Hartree-Fock orbitals are not well suitable for this purpose, since for example σ and π-type orbitals in non-planar molecules may mix significantly. Much better results are obtained if the HF valence orbitals are first localized using the IBO method (the inner-shell orbitals are kept canonical, to avoid any mixing which can affect the correlation energy). This leads to well separated σ and π orbitals, and furthermore allows to select regions for which the orbitals can be frozen in the MCSCF. We then use the frozen IBOs for the inactive space in the MCSCF. Often it is sufficient to optimize only the active space orbitals, which is quite cheap even for larger molecules. Possibly, local inactive orbitals in the vicinity of the active space could be included to achieve higher accuracy. The effect of this approximation is demonstrated for some molecules in Table III. In all cases all inactive orbitals were taken to be HF/IBOs and frozen in the MCSCF optimization, i.e., this is the most extreme approximation. It is found that the CASSCF calculations with the frozen IBO orbitals yield in some cases somewhat too high excitation energies, since the HF/IBO inactive orbitals favor the ground state. However, the errors are largely compensated by the CASPT2 calculations, and then the excitation energies with and without frozen orbitals differ by at most 0.05 eV, which is well below the intrinsic accuracy of CASPT2.

Table IV shows computed vertical excitation energies of the lowest 4 excited states of $[(C_4SH_3)\text{-}[CH_2]_{10}\text{-}(C_4SH_3)]^{2+}$ for various choices of the frozen orbital space. The frozen orbitals were ROHF/IBOs of the lowest triplet state. The geometry and computational details [(10,10) active space, def2-TZVP basis set] have been taken from Ref. 146. In this case the excitation energies are more sensitive to the frozen orbital approximation. If all 77 inactive orbitals are frozen, the CASSCF excitation energies are significantly too high, up to about 1 eV for the third excited state. This error can be strongly reduced by including all valence orbitals of the rings in the optimization, still keeping the $\text{-}[CH_2]_n\text{-}$ chain as well as the C-H bond orbitals of the rings frozen (65 frozen IBOs). Even slightly better results are obtained if the adjacent six C-H and two C-C bond orbitals are also included in the orbital optimization (57 frozen IBOs). The CASSCF excitation energies then agree within less than 0.1 eV with the ones of the fully optimized calculation. Freezing just the core orbitals (28 frozen MOs) has virtually no effect on the results. The PNO-CASPT2 excitation energies are much less sensitive to the frozen orbital approximation, and the results from 0 to 65 frozen core orbitals agree within 0.01-0.02 eV. Even for the calculation with 77 frozen orbitals the errors in the PNO-CASPT2 excitation energies are within 0.07 eV. The total energies can be found in the supporting information.

Guo et al.[146] presented in their paper DLPNO-NEVPT2 excitation energies for $[(C_4SH_3)\text{-}[CH_2]_{30}\text{-}(C_4SH_3)]^{2+}$, and these are compared to our PNO-CASPT2 results in Table V. In the calculation with 145 frozen core all ring valence orbitals were optimized in the CASSCF. In the second set of calculations (137 frozen core orbitals) also the adjacent C-H and C-C bonding orbitals were optimized.

Consistent with the results for $n = 10$, our frozen core CASSCF results are in good agreement with the fully optimized CASSCF values of Guo et al. However, the PNO-CASPT2 excitation energies are lower than the NEVPT2 ones. This is consistent with our experience that that CASPT2 often underestimates valence excitation energies, while NEVPT2 overestimates them (as compared to more accurate MRCI calculations). Small differences in the excitation energies may also be due to the fact that Guo et al. computed the closed-shell Fock matrix without density fitting,[158] while we used in the CASSCF and for the Fock matrix density fitting with the def2-TZVPP/JKFIT basis, and for the remaining integrals in the PNO-CASPT2 the def2-TZVPP/MP2FIT basis. We do not believe, however, that this is the main reason for the differences of CASPT2 and NEVPT2.

TABLE III. CASSCF and CASPT2 calculations using different inactive orbitals (see text). $E^{(1)}$ are the ground state energies in E_h, ΔE the lowest singlet $\pi \rightarrow \pi^*$ vertical excitation energies in eV. The JKFIT and MP2FIT bases which match the orbital bases were used (i.e. AVDZ/JKFIT and AVDZ/MP2FIT with the AVDZ orbital basis). For the PAO domains `IEXT=1` was used.

Molecule	Basis	Orbitals	$E^{(1)}_{\mathrm{REF}}$	$E^{(1)}_{\mathrm{CASPT2}}$	ΔE_{REF}	$\Delta E_{\mathrm{CASPT2}}$	$\Delta E_{\mathrm{LCASPT2}}$
Tryptophan	AVDZ	HF (IBO)	-682.361243	-684.498510	4.666	4.175	4.180
		CASSCF	-682.361633	-684.498855	4.632	4.176	4.181
Tryptophan	AVTZ'	HF (IBO)	-682.509402	-685.074810	4.665	4.114	4.119
		CASSCF	-682.509787	-685.074809	4.630	4.115	4.120
Nicotine	AVDZ	HF(IBO)	-495.842595	-497.508177	5.002	4.569	4.573
		CASSCF	-495.843461	-497.508310	4.855	4.604	4.608
Adrenaline	AVDZ	HF(IBO)	-627.553818	-629.505439	4.824	4.309	4.313
		CASSCF	-627.554067	-629.505687	4.758	4.310	4.313
2Me2HSDiox	AVDZ	HF(IBO)	-856.088906	-857.686883	6.097	4.752	4.757
		CASSCF	-856.089377	-857.687391	5.891	4.801	4.806

TABLE IV. Computed vertical excitation energies for the lowest singlet states of $[(C_4SH_3)\text{-}[CH_2]_{10}\text{-}(C_4SH_3)]^{2+}$ for various numbers of frozen ROHF/IBO orbitals (given over the columns, see text for details). Basis def2-TZVP, default thresholds, (10,10) active space.

	CASSCF					PNO-CASPT2				
State	77	65	57	28	0	77	65	57	28	0
$2\,^1A$	0.889	0.438	0.391	0.362	0.360	0.564	0.533	0.534	0.522	0.520
$3\,^1A$	0.906	0.520	0.482	0.461	0.459	0.564	0.535	0.535	0.525	0.524
$4\,^1A$	1.796	0.958	0.873	0.823	0.819	1.113	1.065	1.067	1.046	1.043
$5\,^1A$	3.730	3.508	3.481	3.418	3.418	3.092	3.053	3.041	3.132	3.131

C. Accuracy

The accuracy of PNO-CASPT2 with respect to the thresholds which determine the PAO and PNO domain sizes has been benchmarked using the molecules in Figure 1. The number of active electrons and orbitals is shown in the figure, and in this test set all active orbitals are of π-type. The geometries (see supporting information) were optimized using MP2 with the AVDZ basis set.

Figure 2 shows the average percentage of correlation energy recovered for all molecules as a function of $T^{\mathrm{occ}}_{\mathrm{PNO}}$, using 3 different choices of PAO domain sizes: `IEXT=1,2` and complete PAO domains (`FULL`). The PAO domain size limits the accuracy that can be achieved with $T^{\mathrm{occ}}_{\mathrm{PNO}} = 0$ (full PNO domains; this corresponds to PAO-CASPT2). Using $T^{\mathrm{occ}}_{\mathrm{PNO}} = 10^{-10}$ and `IEXT=1` about 99.6 % and with `IEXT=2` about 99.9% of the canonical correlation energy are recovered. This is close to the limiting values of the corresponding curves in Fig. 2. With larger PNO occupation number thresholds of 10^{-7} and 10^{-8} about 99.88% and 99.96%, respectively, of the PAO limits are obtained. Based on these results and other tests, we have chosen the default values $T^{\mathrm{occ}}_{\mathrm{PNO}} = 10^{-8}$ and `IEXT=2`, and overall this yields 99.8-99.9% of the canonical correlation energies. This is consistent with what has been found for PNO-LMP2.[99]

The lower limit of the PNO domains for large occupation-number thresholds is determined by the completeness criterion (0.997), and indeed at least 99.7 % of the limiting PAO values are recovered. Interestingly, the average number of PNOs, which is indicated in the figure above the line symbols, is nearly independent of the PAO domain sizes. For the AVDZ basis 50-60 PNOs per pair are required to reach these accuracies.

Figure 3 shows the error of the computed vertical excitation energies (in eV) for the example of tryptophan, again using `IEXT=1,2`, and `FULL` PAO domains. In all cases the errors in the excitation energies are negligibly small, the largest deviation from the canonical result amounts to less than 7 meV. For the default values `IEXT=2` and $T^{\mathrm{occ}}_{\mathrm{PNO}} = 10^{-8}$ the error amounts to 3 meV, which is almost 2 orders of magnitude smaller than the typical intrinsic accuracy of CASPT2.

TABLE V. Comparison of PNO-CASPT2 and DLPNO-NEVPT2 vertical excitation energies for the lowest singlet states of $[(C_4SH_3)\text{-}[CH_2]_{30}\text{-}(C_4SH_3)]^{2+}$. The numbers of frozen inactive orbitals (see text) are given over the columns. Basis def2-TZVP, default thresholds, (10,10) active space.

	CASSCF			CASPT2		NEVPT2
	this work		Ref. 146	this work		Ref. 146
State	145	137	0	145	137	0
$2\,^1A$	0.454	0.408	0.375	0.546	0.547	0.613
$3\,^1A$	0.538	0.500	0.475	0.547	0.548	0.600
$4\,^1A$	0.992	0.908	0.850	1.090	1.092	1.213
$5\,^1A$	3.514	3.488	3.425	2.819	2.991	3.600

FIG. 1. Molecules used to benchmark accuracy of PNO-CASPT2 with active space specifications

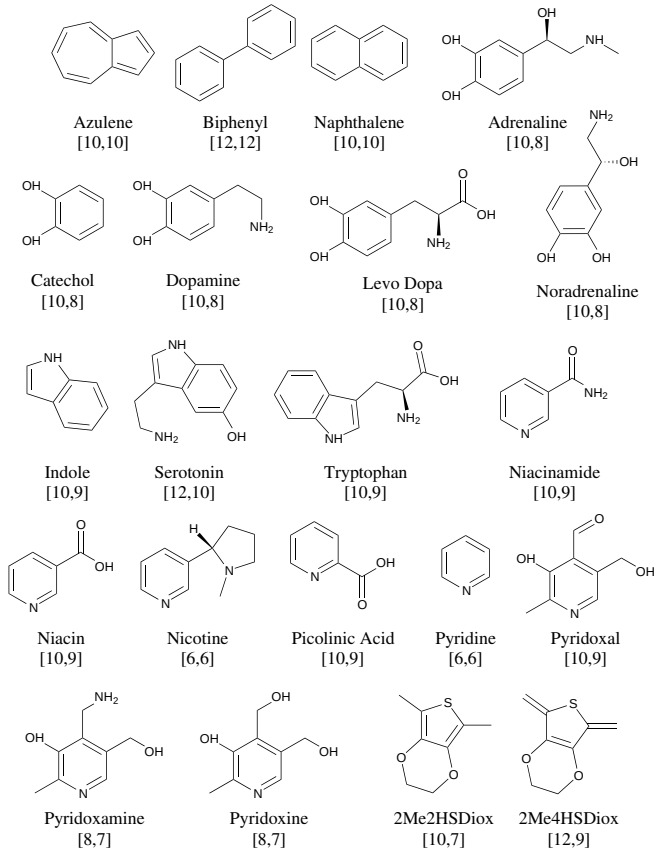

Similar accuracy was achieved for all other molecules, cf. Fig. 4. With the default value of $T_{\mathrm{PNO}}^{\mathrm{occ}} = 10^{-8}$, the maximum errors of the vertical excitation energies for `IEXT=1,2,FULL`, amount to 7, 4, 4 meV, respectively. The errors for `IEXT=1` are mainly determined by the PAO domain size. For `IEXT=2` the errors caused by the PAO and PNO domain approximations become comparable, which shows that our default settings are reasonable.

Fig. 5 shows the convergence of the vertical excitation energy of tryptophan for the AVDZ, AVTZ, and AVQZ basis sets as a function of the domain sizes. The average number of PNOs per pair for a given threshold increases somewhat slower than the number of basis functions. For example, for $T_{\mathrm{PNO}}^{\mathrm{occ}} = 10^{-8}$ the ratio of the average domain size to the basis set size is 0.325 for AVDZ and 0.227 for AVQZ. The domain errors for a given threshold are comparable for all basis sets. The effect of the basis on the vertical excitation energies is small, the canonical AVDZ and AVQZ values only differ by 0.071 eV. Similar results were also obtained for some other molecules. Of course, the basis set dependency may be more pronounced for charge-transfer states or higher excited states, in particular for Rydberg states.

D. Efficiency and scaling with molecular size

1. Scaling

In order to demonstrate the asymptotic scaling of the computational cost with molecular size, we use the $[(C_4SH_3)\text{-}[CH_2]_n\text{-}(C_4SH_3)]^{2+}$ biradical system from the

FIG. 2. Convergence of the average correlation energies of the molecules in Fig. 1 (in % of the canonical value) as a function of $T_{\mathrm{PNO}}^{\mathrm{occ}}$ for various PAO domain sizes (`IEXT=1,2` and `FULL` domains). The AVDZ basis has been used. The numbers above the symbols are the average PNO domain sizes.

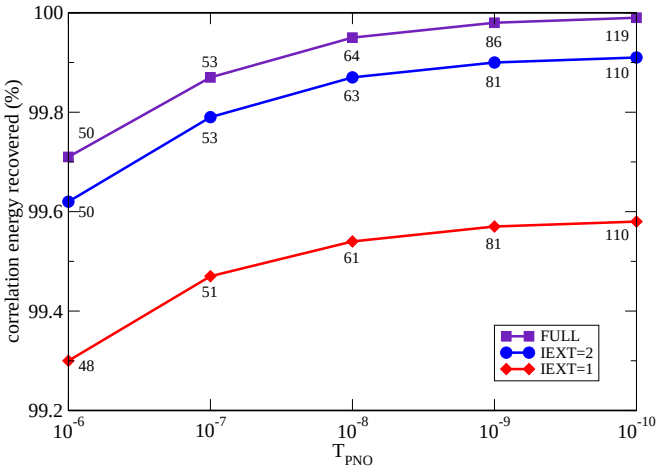

work of Guo et al.[146] The geometries have been taken from the supporting information of that paper and the same active space (10 electrons in 10 π-orbitals) and orbital basis set (def2-TZVP) has been used. The orbitals were optimized in state-averaged CASSCF calculations, including 5 singlet and 5 triplet states. For the longer chains singlets and triplets become degenerate, and for technical reasons the orbitals were optimized separately for singlets and triplets (which does not affect the energies). At the time when we did these calculations we thought that SA-CASSCF orbitals for 5 singlet and 5 triplet states were used by Guo et al. throughout their paper (as in their Table 5), but after submission of our manuscript we were informed that they included only one singlet and one triplet state in their scaling test calculations.[158] Since the choice of orbitals should not affect the timings, we did not repeat the calculations. In order to avoid excessive MCSCF optimization times, we used ROHF/IBO frozen inactive orbitals of the triplet state in the final calculations for all n. This is irrelevant for the CASPT2 timings but affects the excitation energies, as has already been demonstrated in IV B.

Fig. 6 shows the dependence of the CPU times of the dominant parts of the calculation as a function of the chain length n, using 1 compute core of a Xeon E5-2660 v3 @ 2.60GHz processor. The timings for singlets and triplets are almost the same, and therefore only results for the singlets will be presented. The scaling is very close to linear, and the largest calculation for $n = 50$ (166 atoms, 2508 basis functions) took 17 minutes. This may be compared with Fig. 6 or Ref. 146, which indicates that the DLPNO-NEVPT2 calculation with the same basis set on one compute core took about 170 min (using one core on a Xeon E5649 2.53 GHZ processor). Of course, such comparisons with different hardware give only a rough indication of the relative performance.

FIG. 3. Convergence of the average error in the vertical excitation energies of tryptophan (in meV relative to the canonical values) as a function of T_{PNO}^{occ} for various PAO domain sizes (`IEXT=1,2` and `FULL` domains). The AVDZ basis has been used.

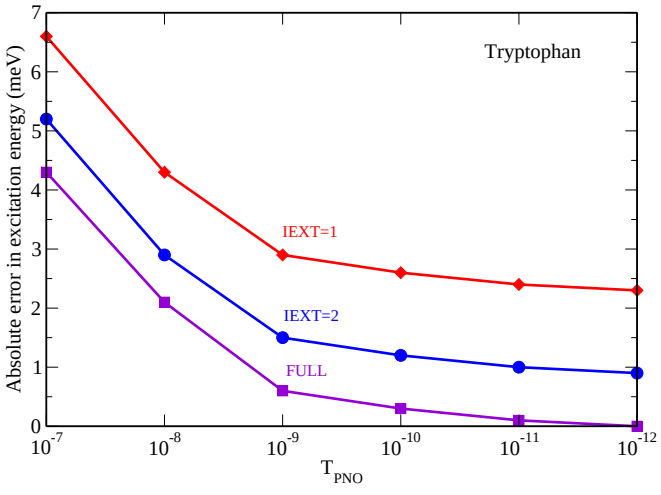

FIG. 4. Absolute Errors of vertical excitation energies (in eV) for the default threshold $T_{\mathrm{PNO}}^{\mathrm{occ}} = 10^{-8}$, $T_{\mathrm{PNO}}^{\mathrm{en}} = 0.997$ relative to the canonical values using different PAO thresholds (`IEXT=1,2,FULL`).

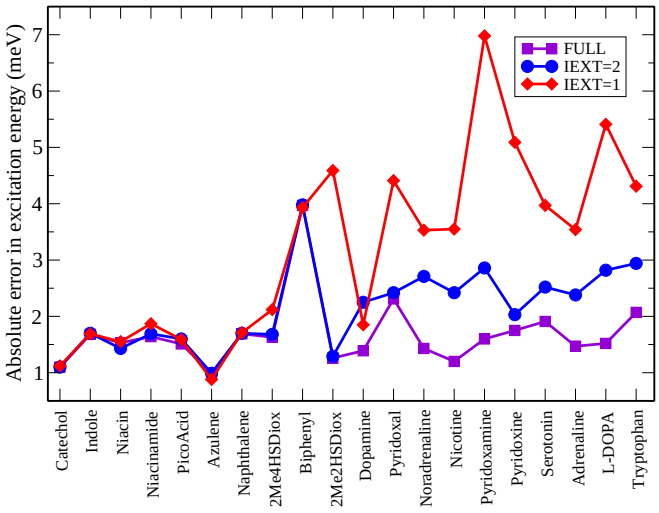

FIG. 5. Errors of vertical excitation energies of tryptophan relative to the canonical values as a function of the average PNO domain size for 3 different basis sets. Default PAO domain sizes were used. The numbers in the figure correspond to the PNO thresholds for the first 3 points from the left. The canonical CASPT2 reference values for the AVDZ, AVTZ, and AVQZ basis sets are 4.176, 4.113, and 4.105 eV, respectively.

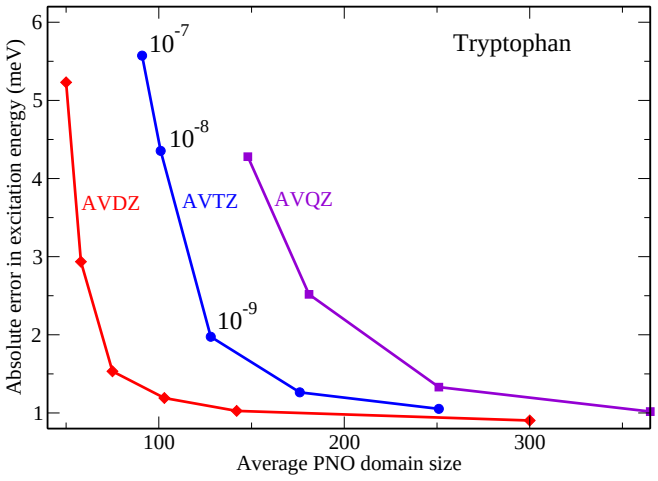

The times needed to compute the residuals for the individual subspaces are shown in Fig. 7 as a function of the chain length n. As expected, most time is spent for computing the P_2 residuals. This time increases linearly with the molecular size. The times for the remaining spaces are nearly independent of n; this is due to the restriction that the corresponding inactive indices i and/or j must be close to the active space. As mentioned before, this approximation affects the energy of the largest chain only

FIG. 6. Timings of PNO-CASPT2 calculations for the ^1A ground states of $[(C_4SH_3)\text{-}[CH_2]_n\text{-}(C_4SH_3)]^{2+}$ using SA-CASSCF (10,10) reference functions (see text). One compute core of a Xeon E5-2660 v3@2.60GHz processor was used.

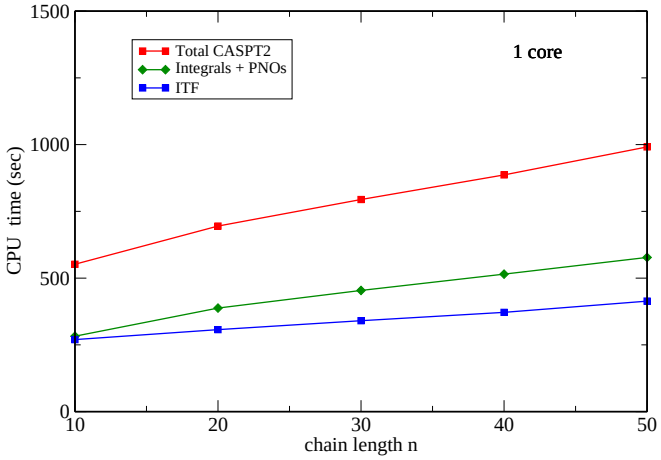

FIG. 7. Timings of PNO-CASPT2 calculations for individual contributions to the PNO-CASPT2 residuals for the same systems as in Fig. 6. The timings refer to 7 iterations.

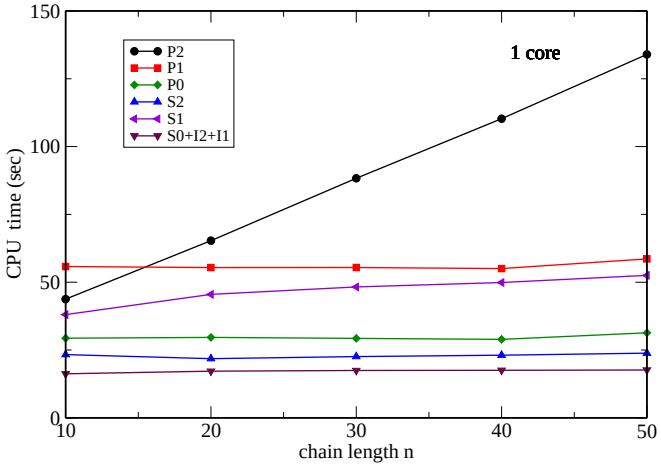

by about 10 μH. The large fraction of iteration time that is independent of the molecular size explains the slow increase of the total time with chain length in Fig. 6.

2. Application to copper and iron complexes

To demonstrate the applicability of the method to larger systems, we carried out calculations for the singlet and triplet side-on Cu - O_2 complexes with the L^2 ligand from the work of Gherman et al.[159], and for a $FeC_{72}N_2H_{100}$ complex from Guo et al.[146] The geometries were taken from the respective papers and are shown schematically in Fig. 8.

For the Fe-complex the same basis set (def2-TZVP) and active space (6,5) as in the NEVPT2 calculations of Guo

FIG. 8. The Cu and Fe-complex

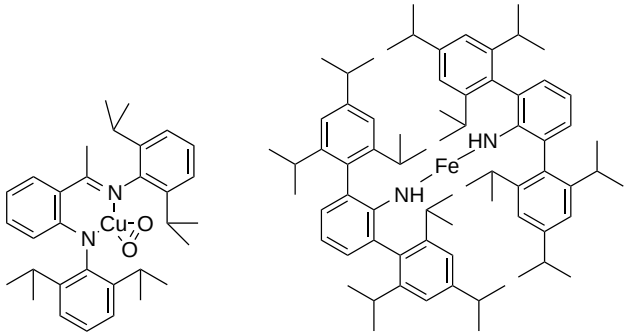

Cu complex from Ref. 159 Fe-complex from Ref. 146

et al. were used (2939 basis functions, 406 correlated electrons, 10999 non-distant orthogonal pairs). The computed total energies of the quintet ground state of the Fe-complex as well as the energy differences to the triplet and singlet excited states are presented in Table VI and compared with DLPNO-NEVPT2 calculations of Guo et al.[146] The CASSCF energies of both calculations slightly differ, since Guo et al. used state-averaged CASSCF optimization for the lowest two states and did not use density fitting to compute the closed-shell part of the Fock matrix.[158] In our CASSCF calculations we optimized the states separately and only optimized the 9 orbitals that are exclusively localized at the Fe and neighboring N atoms (based on IBO partial charges). The remaining 279 orbitals were frozen ROHF/IBO orbitals of the ^5A ground state. For this state the ROHF energy is identical to the ground state CASSCF energy. Thus, the freezing approximation only affects the excited states, and this may partly explain why our CASSCF excitation energy to the triplet state is slightly higher than the one of Guo et al. For comparison, a second set of CASSCF calculations was carried out, in which all 13 IBOs that contain the Fe and N atoms were optimized. This lowers the CASSCF excitation energies for the ^3A and ^1A states by only 0.004 and 0.003 eV, respectively. The IBO subspaces of 9 or 13 orbitals that were optimized in the CASSCF were chosen automatically using the region method described in Ref. 63, and correspond to the "exclusive" and "inclusive" options in `MOLPRO`, respectively.

As already mentioned, our PNO-CASPT2 excitation energy for the ^3A state is somewhat higher than the DLPNO-NEVPT2 one, and our computed correlation energy with level shift 0.3 E_h, `IEXT=1` is 1.2% smaller. As shown in Table VII, the latter result is mainly due to the level shift; if the shift is reduced to 0.1 E_h and `IEXT` is increased to 2, we obtain a ground-state correlation energy that is almost identical to the NEVPT2 value of Guo at al. However, the excitation energies are hardly affected by the level shift and the PAO domain size (`IEXT`). Part of the difference in the excitation energy may also be due to the fact that we optimized the orbitals for each

TABLE VI. First line: CASSCF total energies (+4156 E_h) and CASPT2/NEVPT2 correlation energies (in E_h) for the ^5A ground state of the $FeC_{72}N_2H_{100}$ complex. Other lines: vertical excitation energies (in eV) .

State	CASSCF		CASPT2	NEVPT2
	this work[a]	Ref. 146	this work[b]	Ref. 146
^5A	-0.160061	-0.158509	-12.174903	-12.314239
^3A	2.265	2.124	2.160	1.852
^1A	3.586	-	3.276	-

Using 279 frozen HF/IBO inactive orbitals, see text.
Using level shift of 0.3 E_h and `IEXT=1`, see text.

TABLE VII. PNO-CASPT2 correlation energies for the ^5A ground state (in E_h) and excitation energies (in eV) of the $FeC_{72}N_2H_{100}$ complex using different level shifts and PAO domain sizes. The reference function is the same as in table VI.

Shift[a]	IEXT	$E_{corr}(^5A)$	$\Delta E(^3A)$	$\Delta E(^1A)$	CPU-time[b]
0.1	1	-12.272074	2.134	3.163	2239
0.1	2	-12.314300	2.120	3.146	4522
0.3	1	-12.174884	2.160	3.276	1973
0.3	2	-12.216587	2.146	3.263	4230

a) Calculations without level shift did not converge.
b) Using 4 cores of a Xeon E5-2660 v3@2.60GHz processor.

state separately, while Guo et al. used state-averaged orbitals. These differences became only clear when this manuscript was completed.[158]

For the Cu-complex the basis set was aug-cc-pVTZ for the oxygen atoms, cc-pVTZ-PP with ECP10MDF effective core potential for Cu, and cc-pVTZ for all other atoms (1749 contracted basis functions, 202 correlated electrons, 4322 non-distant pairs). In the CASSCF calculations we optimized the Cu($3d$) and O_2 valence orbitals, as well as all orbitals which contain the adjacent nitrogen atoms in the primary orbital domains. All other 122 orbitals were frozen ROHF/IBOs of the triplet state at the corresponding geometry. Since the singlet state has strong multi-reference character and is not well described by closed-shell HF orbitals, we used triplet ROHF frozen core orbitals for both states. For comparison, we also carried out calculations in which all valence orbitals were optimized in the CASSCF, and only the 40 inner-shell core orbitals were frozen.

The electronic structure of the Cu complexes in the lowest singlet and triplet states can be roughly described as $L^-\ Cu^{2+}\ O_2^-$. For the following discussion we assume that the Cu-O_2 group lies in the xy-plane, with O_2 oriented parallel to the x-axis. The O_2 π_y orbitals in the xy plane will be denoted $\pi_\parallel$, and $\pi^*_\parallel$, the π_z ones perpendicular to the plane as $\pi_\perp$ and $\pi^*_\perp$ (the π and π^* orbitals correspond to the bonding π_u and antibonding π_g orbitals of the free O_2 molecule, respectively). Our active spaces further include the molecular O_2 $3\sigma_g$ and $3\sigma_u$ orbitals, which in the complex will be denoted as 3σ and $3\sigma^*$ (the latter being weakly occupied).

In both states one electron is transferred from the Cu($3d_{xy}$) orbital to an $O_2(\pi^*)$ orbital. In the singlet state, the transfer occurs to the $\pi^*_\perp$ orbital, which then becomes doubly occupied. The singly occupied Cu($3d_{xy}$) and $\pi^*_\parallel$ orbitals then form a $d-\pi$ bond. However, this has significant biradical character, and the leading configurations in which either the bonding or antibonding orbitals are doubly occupied have coefficients of about 0.8 and 0.4, respectively. In the triplet state the transfer occurs from Cu($3d_{xy}$) to the $\pi^*_\parallel$ orbital. The state can thus be described as $^3(d_{xy}\ \pi^*_\perp)$ and has pure single reference character. State-averaged CASSCF calculations showed that the corresponding $^3(d_{xy}\ \pi^*_\parallel)$ state is considerably higher in energy. In agreement with experimental and previous theoretical findings,[159,160] our calculations predict the singlet state be the ground state, about 20 kcal mol^{-1} lower then the triplet state (see below).

We tested various active spaces. In all cases the orbitals for the singlet and triplet states (which have different equilibrium geometries) were optimized separately. Most consistent orbitals were obtained with a small active space with 6 electrons in 5 orbitals [for the singlet $(3d_{xy}, 3\sigma, 3\sigma^*, \pi_\parallel, \pi^*_\parallel)$ and for the triplet $(3d_{xy}, 3\sigma, 3\sigma^*, \pi_\perp, \pi^*_\perp)$]. This yields a CASPT2 singlet-triplet splitting $\Delta E_{ST} = E_T - E_S$ of 20.2 kcal mol^{-1}. Calculations which included more strongly occupied orbitals in the active space (e.g. with 9, 11, or 13 active orbitals, which comprise all O_2 valence orbitals and either 1, 3, or 5 Cu($3d$) orbitals) gave similar results. For example our CASPT2 calculations with the (18,11) active space and 122 frozen ROHF/IBO orbitals yielded Δ_{ST} = 19.2 kcal mol[1], while a calculation in which all valence orbitals were optimized (40 frozen core orbitals) yielded 20.3 kcal mol^{-1}. However, since the occupation numbers of the additional orbitals were very close to 2, significant mixing with contributions from other atoms occurred, and the active orbitals for the two states were less consistent than with the small active space. Further calculations for the side-on and end-on Cu-complexes are under way and will be reported elsewhere.

Timings of the individual steps for these complexes are presented in Table VIII, using 4 compute cores. For comparison, the timings for the linear $[(C_4SH_3)$-$[CH_2]_{50}$-$(C_4SH_3)]^{2+}$ model system are also included. Using 4 cores, the CASPT2 calculations for the linear chain took only 6 minutes, the ones for the singlet ground state of the Cu-complex with the (6,5) and (18,11) active spaces 9 and 13 minutes, respectively, and the one for Fe-complex 33 minutes. Most time is needed to compute the integrals and for the iterations; the more dense and 3-dimensional the molecule, the larger is the fraction of time required for the integrals. The exact memory requirements are difficult to determine, but all calculations could be done using

8 GB of dynamically allocated work space per core. In addition, about 40 GB of global array space were needed for the calculation of the Fe-complex.

V. CONCLUSIONS

We have described the theory and implementation of a local PNO-CASPT2 method. The configuration space is fully internally contracted. It is demonstrated that the computational effort for extended systems scales linearly with molecular size, provided that the active space is local. But even for medium size molecules, where the linear scaling regime is not reached, the local approximations lead to a drastic reduction of the computation time, memory, and disk space.

The integral evaluation and PNO generation are very well parallelized, similar as in our previous single-reference PNO-LMP2 and PNO-LMP2-F12 methods.[99,100] However, the iterative solution of the CASPT2 amplitude equations, which is implemented using the local integrated tensor framework, is only partly parallelized, and therefore the overall speedups are still limited to a factor of 3-4. Work is in progress to improve the parallelization and make the method applicable on distributed memory multi-node compute clusters.

The orthogonalization of the internally contracted configurations requires that the theory is invariant with respect to unitary transformations within the active space, and therefore a single PAO domain is used for the active space. The PNO domains for P_0 pairs are still pair-specific, but since the pairs are uniquely defined the results are independent of unitary transformations among the initial active orbitals.

The accuracy of the method has been evaluated by comparing correlation energies and vertical excitation energies with corresponding canonical calculations. With default thresholds for the PAO and PNO domain sizes, about 99.9% of the canonical correlation energies are recovered. The excitation energies were found to be very insensitive to the domain sizes, and even with rather coarse thresholds the domain errors are below 0.1 eV.

A major problem is the definition of the active space and the optimization of the HF and CASSCF reference functions for large molecules. Usually, the full orbital optimization takes much longer than the PNO-CASPT2 calculations. In order to restrict the active space to the desired region and at the same time drastically reduce the computational cost for the optimization, we have proposed to use frozen HF/IBOs for part of the inactive space or even all inactive orbitals. It has been found that the changes of the CASPT2 excitation energies caused by frozen inactive orbitals are small. A more detailed investigation of such approximation and procedures is currently under way in our laboratory. Additionally, the computation of the Fock matrix in CASSCF calculations can be speeded up using local density fitting approximations, similarly to the Hartree-Fock method[161,162], and we are currently working on a new MCSCF method that is suitable to treat large molecules.

So far, our PNO-CASPT2 method is state specific and - as any other single-state CASPT2 method - does not allow for a relaxation of the reference function. We plan to implement a multi-state version in the future. Furthermore, we see this work as the first step in developing more accurate local multi-reference coupled-cluster methods which are applicable to large molecular systems.

ACKNOWLEDGEMENTS

This work has been funded by the ERC Advanced Grant 320723 (ASES).

[1] B. O. Roos, P. Linse, P. E. M. Siegbahn, and M. R. A. Blomberg, Chem. Phys. **66**, 197 (1982).
[2] K. Andersson, P.-Å. Malmqvist, B. O. Roos, A. J. Sadlej, and K. Wolinski, J. Phys. Chem. **94**, 5483 (1990).
[3] K. Andersson, P. A. Malmqvist, and B. O. Roos, J. Chem. Phys. **96**, 1218 (1992).
[4] J. Finley, P. Å. Malmqvist, B. O. Roos, and L. Serrano-Andrés, Chem. Phys. Lett. **288**, 299 (1998).
[5] T. Shiozaki and H.-J. Werner, Mol. Phys. **111**, 607 (2013).
[6] T. Shiozaki, W. Győrffy, P. Celani, and H.-J. Werner, J. Chem. Phys. **135**, 081106 (2011).
[7] P. Celani and H.-J. Werner, J. Chem. Phys. **119**, 5044 (2003).
[8] W. Győrffy, T. Shiozaki, G. Knizia, and H.-J. Werner, J. Chem. Phys. **138**, 104104 (2013).
[9] S. Ten-no, Chem. Phys. Lett. **447**, 175 (2007).
[10] T. Shiozaki and H.-J. Werner, J. Chem. Phys. **133**, 141103 (2010).
[11] T. Shiozaki, G. Knizia, and H.-J. Werner, J. Chem. Phys. **134**, 034113 (2011).
[12] T. Shiozaki and H.-J. Werner, J. Chem. Phys. **134**, 184104 (2011).
[13] F. Aquilante, P.-A. Malmqvist, T. B. Pedersen, A. Ghosh, and B. O. Roos, J. Chem. Theory Comput. **4**, 694 (2008).
[14] K. Wolinski and P. Pulay, J. Chem. Phys. **90**, 3647 (1989).
[15] K. Andersson, Theoretical Chemistry Accounts **91**, 31 (1995).
[16] K. G. Dyall, J. Chem. Phys. **102**, 4909 (1995).
[17] G. Ghigo, B. Roos, and P. Malmqvist, Chem. Phys. Lett. **396**, 142 (2004).
[18] B. O. Roos and K. Andersson, Chem. Phys. Lett. **245**, 215 (1995).
[19] C. Angeli, R. Cimiraglia, S. Evangelisti, T. Leininger, and J. P. Malrieu, J. Chem. Phys. **114**, 10252 (2001).
[20] C. Angeli, R. Cimiraglia, and J. P. Malrieu, J. Chem. Phys. **117**, 9138 (2002).
[21] C. Angeli, B. Bories, A. Cavallini, and R. Cimiraglia, J. Chem. Phys. **124**, 054108 (2006).
[22] R. W. A. Havenith, P. R. Taylor, C. Angeli, R. Cimiraglia, and K. Ruud, J. Chem. Phys. **120**, 4619 (2004).
[23] C. Angeli, S. Borini, M. Cestari, and R. Cimiraglia, J. Chem. Phys. **121**, 4043 (2004).
[24] C. Angeli, M. Pastore, and R. Cimiraglia, Theor. Chem. Acc. **117**, 743 (2007).
[25] M. F. Rode and H.-J. Werner, Theoretical Chemistry Accounts **114**, 309 (2005).
[26] H.-J. Werner, Mol. Phys. **89**, 645 (1996).
[27] P. E. M. Siegbahn, J. Chem. Phys. **72**, 1647 (1980).

TABLE VIII. CPU times (in sec)[a] for the dominant parts of PNO-CASPT2 calculations (`IEXT=1`).

Step	Ch50	Cu-com[b]	Fe-com	Remarks
Density matrices:	1	0	0	includes all density matrices and the quantities in eqs. (79)-(82)
SC-PAO domains:	36	47	107	includes calculation of PAOs, domain generation and ICC orthogonalization
PAO(SC) Integrals:	102	224	1128	includes transformations to orthogonal ICC basis
PNO generation:	17	25	52	includes integral transformation from PAO(SC) to PNO basis
ITF initialization:	6	3	12	set up pair and address lists
ITF intermediates:	35	34	91	includes PNO overlap matrix
ITF solve:	157	188	574	Cu-complex 9 iterations, others 7 iterations.
Total:	365	524	1973	does not include CASSCF calculation of the reference function

a) Using 4 cores of a Xeon E5-2660 v3@2.60GHz node with 20 cores and 256 GB of memory

b) Singlet state with (6,5) active space, see text.

[28] V. R. Saunders and J. H. van Lenthe, Mol. Phys. **48**, 923 (1983).
[29] R. Fink and V. Staemmler, Theor. Chem. Acc. **87**, 129 (1993).
[30] T. J. Martinez and E. A. Carter, J. Chem. Phys. **102**, 7564 (1995).
[31] H.-J. Werner and P. J. Knowles, J. Chem. Phys. **89**, 5803 (1988).
[32] P. J. Knowles and H.-J. Werner, Chem. Phys. Lett. **145**, 514 (1988).
[33] H.-J. Werner and P. J. Knowles, Theoretical Chemistry Accounts **78**, 175 (1990).
[34] P. J. Knowles and H.-J. Werner, Theor. Chem. Acc. **84**, 95 (1992).
[35] P. Celani, H. Stoll, H.-J. Werner, and P. J. Knowles, Mol. Phys. **102**, 2369 (2004).
[36] K. R. Shamasundar, G. Knizia, and H.-J. Werner, J. Chem. Phys. **135**, 054101 (2011).
[37] U. S. Mahapatra, B. Datta, B. Bandyopadhyay, and D. Mukherjee, Adv. Quant. Chem. **30**, 163 (1998).
[38] F. A. Evangelista, M. Hanauer, A. Köhn, and J. Gauss, J. Chem. Phys. **136**, 204108 (2012).
[39] M. Hanauer and A. Köhn, Chem. Phys. **401**, 50 (2012).
[40] M. Hanauer and A. Köhn, J. Chem. Phys. **137**, 131103 (2012).
[41] M. Hanauer and A. Köhn, J. Chem. Phys. **136**, 204107 (2012).
[42] P. Pulay, Chem. Phys. Lett. **100**, 151 (1983).
[43] S. Saebø and P. Pulay, Chem. Phys. Lett. **113**, 13 (1985).
[44] P. Pulay and S. Saebø, Theor. Chim. Acta **69**, 357 (1986).
[45] S. Saebø and P. Pulay, J. Chem. Phys. **86**, 914 (1987).
[46] S. Saebø and P. Pulay, J. Chem. Phys. **88**, 1884 (1988).
[47] S. Saebø and P. Pulay, Annu. Rev. Phys. Chem. **44**, 213 (1993).
[48] C. Hampel and H.-J. Werner, J. Chem. Phys. **104**, 6286 (1996).
[49] G. Hetzer, P. Pulay, and H.-J. Werner, Chem. Phys. Lett. **290**, 143 (1998).
[50] G. Hetzer, M. Schütz, H. Stoll, and H.-J. Werner, J. Chem. Phys. **113**, 9443 (2000).
[51] M. Schütz, G. Hetzer, and H.-J. Werner, J. Chem. Phys. **111**, 5691 (1999).
[52] M. Schütz and H.-J. Werner, Chem. Phys. Lett. **318**, 370 (2000).
[53] M. Schütz, J. Chem. Phys. **113**, 9986 (2000).
[54] M. Schütz and H.-J. Werner, J. Chem. Phys. **114**, 661 (2001).
[55] M. Schütz, J. Chem. Phys. **116**, 8772 (2002).
[56] M. Schütz, Phys. Chem. Chem. Phys. **4**, 3941 (2002).
[57] H.-J. Werner, F. R. Manby, and P. Knowles, J. Chem. Phys. **118**, 8149 (2003).
[58] M. Schütz, H.-J. Werner, R. Lindh, and F. R. Manby, J. Chem. Phys. **121**, 737 (2004).
[59] M. Schütz and F. R. Manby, Phys. Chem. Chem. Phys. **5**, 3349 (2003).
[60] H.-J. Werner and K. Pflüger, Ann. Reports in Comput. Chem. **2**, 53 (2006).
[61] R. Mata and H.-J. Werner, J. Chem. Phys. **125**, 184110 (2006).
[62] R. Mata and H.-J. Werner, Mol. Phys. **105**, 2753 (2007).
[63] R. Mata, H.-J. Werner, and M. Schütz, J. Chem. Phys. **128**, 144106 (2008).
[64] H.-J. Werner and M. Schütz, J. Chem. Phys. **135**, 144116 (2011).
[65] D. Kats and F. R. Manby, J. Chem. Phys. **138**, 144101 (2013).
[66] D. Kats, J. Chem. Phys. **141**, 244101 (2014).
[67] D. Kats and M. Schütz, J. Chem. Phys. **131**, 124117 (2009).
[68] K. Freundorfer, D. Kats, T. Korona, and M. Schütz, J. Chem. Phys. **133**, 244110 (2010).
[69] P. E. Maslen and M. Head-Gordon, Chem. Phys. Lett. **283**, 102 (1998).
[70] P. E. Maslen and M. Head-Gordon, J. Chem. Phys. **109**, 7093 (1998).
[71] P. Y. Ayala and G. E. Scuseria, J. Chem. Phys. **110**, 3660 (1999).
[72] G. E. Scuseria and P. Y. Ayala, J. Chem. Phys. **111**, 8330 (1999).
[73] P. E. Maslen, A. Dutoi, M. S. Lee, Y. H. Shao, and M. Head-Gordon, Mol. Phys. **103**, 425 (2005).
[74] N. J. Russ and T. D. Crawford, Chem. Phys. Lett. **400**, 104 (2004).
[75] R. A. DiStasio, Y. S. Jung, and M. Head-Gordon, J. Chem. Theory Comput. **1**, 862 (2005).
[76] J. E. Subotnik and M. Head-Gordon, J. Chem. Phys. **123**, 064108 (2005).
[77] A. Auer and M. Nooijen, J. Chem. Phys. **125**, 024104 (2006).
[78] K. V. Lawler, J. A. Parkhill, and M. Head-Gordon, Mol. Phys. **106**, 2309 (2008).
[79] T. S. Chwee, A. B. Szilva, R. Lindh, and E. A. Carter, J. Chem. Phys. **128**, 224106 (2008).
[80] B. Doser, D. S. Lambrecht, J. Kussmann, and C. Ochsenfeld, J. Chem. Phys. **130**, 064107 (2009).
[81] S. A. Maurer, L. Clin, and C. Ochsenfeld, J. Chem. Phys. **140**, 224112 (2014).
[82] H. F. Schurkus and C. Ochsenfeld, J. Chem. Phys. **144**, 031101 (2016).
[83] F. Neese, F. Wennmohs, and A. Hansen, J. Chem. Phys. **130**, 114108 (2009).
[84] F. Neese, A. Hansen, and D. G. Liakos, J. Chem. Phys. **131**, 064103 (2009).
[85] A. Hansen, D. G. Liakos, and F. Neese, J. Chem. Phys. **135**, 214102 (2011).
[86] D. G. Liakos, A. Hansen, and F. Neese, J. Chem. Theory Comput. **7**, 76 (2011).
[87] R. Izsak, A. Hansen, and F. Neese, Mol. Phys. **110**, 2413 (2012).
[88] C. Riplinger and F. Neese, J. Chem. Phys. **138**, 034106 (2013).
[89] C. Riplinger, B. Sandhoefer, A. Hansen, and F. Neese, J. Chem. Phys. **139**, 134101 (2013).
[90] P. Pinski, C. Riplinger, E. F. Valeev, and F. Neese, J. Chem. Phys. **143**, 034108 (2015).

[91] C. Riplinger, P. Pinski, U. Becker, E. F. Valeev, and F. Neese, J. Chem. Phys. **144**, 024109 (2016).
[92] M. Schwilk, D. Usvyat, and H.-J. Werner, J. Chem. Phys. **142**, 121102 (2015).
[93] C. Edmiston and M. Krauss, J. Chem. Phys. **42**, 1119 (1965).
[94] W. Meyer, Int. J. Quantum Chem. **5**, 341 (1971).
[95] W. Meyer, J. Chem. Phys. **58**, 1017 (1973).
[96] R. Ahlrichs, F. Driessler, H. Lischka, V. Staemmler, and W. Kutzelnigg, J. Chem. Phys. **62**, 1235 (1975).
[97] C. Krause and H.-J. Werner, Phys. Chem. Chem. Phys. **14**, 7591 (2012).
[98] C. Hättig, D. P. Tew, and B. Helmich, J. Chem. Phys. **136**, 204105 (2012).
[99] H.-J. Werner, G. Knizia, C. Krause, M. Schwilk, and M. Dornbach, J. Chem. Theory Comput. **11**, 484 (2015).
[100] Q. Ma and H.-J. Werner, J. Chem. Theory Comput. **11**, 5291 (2015).
[101] H.-J. Werner and F. R. Manby, J. Chem. Phys. **124**, 054114 (2006).
[102] H.-J. Werner, J. Chem. Phys. **129**, 101103 (2008).
[103] T. B. Adler, H.-J. Werner, and F. R. Manby, J. Chem. Phys. **130**, 054106 (2009).
[104] T. B. Adler and H.-J. Werner, J. Chem. Phys. **130**, 241101 (2009).
[105] T. B. Adler and H.-J. Werner, J. Chem. Phys. **135**, 144117 (2011).
[106] F. Pavošević, P. Pinski, C. Riplinger, F. Neese, and E. F. Valeev, J. Chem. Phys. **144**, 144109 (2016).
[107] D. G. Fedorov and K. Kitaura, J. Chem. Phys. **123**, 134103 (2005).
[108] T. F. Hughes, N. Flocke, and R. J. Bartlett, J. Phys. Chem. A **112**, 5994 (2008).
[109] W. Li, P. Piecuch, J. R. Gour, and S. Li, J. Chem. Phys. **131**, 114109 (2009).
[110] W. Li and P. Piecuch, J. Phys. Chem. A **114**, 8644 (2010).
[111] W. Li and P. Piecuch, J. Phys. Chem. A **114**, 6721 (2010).
[112] W. Li, Y. Guo, and S. Li, Phys. Chem. Chem. Phys. **14**, 7854 (2012).
[113] M. Ziółkowski, B. Jansìk, T. Kjærgaard, and P. Jørgensen, J. Chem. Phys. **133**, 014107 (2010).
[114] K. Kristensen, M. Ziółkowski, B. Jansìk, T. Kjærgaard, and P. Jørgensen, J. Chem. Theory Comput. **7**, 1677 (2011).
[115] K. Kristensen, P. Jørgensen, B. Jansìk, T. Kjærgaard, and S. Reine, J. Chem. Phys. **137**, 114102 (2012).
[116] I.-M. Høyvik, K. Kristensen, B. Jansìk, and P. Jørgensen, J. Chem. Phys. **136**, 014105 (2012).
[117] K. Kristensen, T. Kjærgaard, I.-M. Høyvik, P. Ettenhuber, P. Jørgensen, B. Jansik, S. Reine, and J. Jakowski, Mol. Phys. **111**, 1196 (2013).
[118] Z. Rolik and M. Kallay, J. Chem. Phys. **135**, 104111 (2011).
[119] Z. Rolik, L. Szegedy, I. Ladjánszki, B. Ladóczki, and M. Kallay, J. Chem. Phys. **139**, 094105 (2013).
[120] H. Stoll, J. Chem. Phys. **97**, 8449 (1992).
[121] J. Friedrich, M. Hanrath, and M. Dolg, J. Chem. Phys. **126**, 154110 (2007).
[122] J. Friedrich and M. Dolg, J. Chem. Phys. **129**, 244105 (2008).
[123] J. Friedrich, S. Coriani, T. Helgaker, and M. Dolg, J. Chem. Phys. **131**, 154102 (2009).
[124] J. Friedrich and M. Dolg, J. Chem. Theory Comput. **5**, 287 (2009).
[125] O. R. Meitei and A. Hesselmann, J. Chem. Phys. **144**, 084109 (2016).
[126] S. Hoyau, D. Maynau, and J.-P. Malrieu, J. Chem. Phys. **134**, 054125 (2011).
[127] D. Walter, A. Venkatnathan, and E. Carter, J. Chem. Phys. **118**, 8127 (2003).
[128] D. B. Krisiloff and E. A. Carter, Phys. Chem. Chem. Phys. **14**, 7710 (2012).
[129] D. B. Krisiloff, C. M. Krauter, F. J. Ricci, and E. A. Carter, J. Chem. Theory Comput. **11**, 5242 (2015).
[130] H. Lischka, R. Shepard, F. B. Brown, and I. Shavitt, Int. J. Quant. Chem. **20**, 91 (1981).
[131] T. S. Chwee and E. A. Carter, Mol. Phys. **108**, 2519 (2010).
[132] T. S. Chwee and E. A. Carter, J. Chem. Phys. **132**, 074104 (2010).
[133] O. Demel, J. Pittner, and F. Neese, J. Chem. Theory Comput. **11**, 3104 (2015).
[134] W. Meyer, "Modern theoretical chemistry vol. 3," (Plenum, New York, 1977) Chap. Configuration Expansion by Means of Pseudonatural Orbitals.
[135] P. E. M. Siegbahn, Int. J. Quant. Chem. **18**, 1229 (1980).
[136] H.-J. Werner and E. A. Reinsch, Proceedings of the fifth seminar on computational methods in quantum chemistry, Groningen, Holland (1981).
[137] H.-J. Werner and E. A. Reinsch, J. Chem. Phys. **76**, 3144 (1982).
[138] T. Yanai and G. K. L. Chan, J. Chem. Phys. **124**, 194106 (2006).
[139] T. Yanai and G. K. L. Chan, J. Chem. Phys. **127**, 104107 (2007).
[140] G. K. L. Chan and T. Yanai, Adv. Chem. Phys. **134**, 343 (2007).
[141] E. Neuscamman, T. Yanai, and G. K. L. Chan, J. Chem. Phys. **130**, 124102 (2009).
[142] E. Neuscamman, T. Yanai, and G. K. L. Chan, J. Chem. Phys. **132**, 024106 (2010).
[143] T. Yanai, Y. Kurashige, E. Neuscamman, and G. K. L. Chan, J. Chem. Phys. **132**, 024105 (2010).
[144] P. Celani and H.-J. Werner, J. Chem. Phys. **112**, 5546 (2000).
[145] H.-J. Werner, P. J. Knowles, G. Knizia, F. R. Manby, and M. Schütz, WIREs Comput Mol Sci **2**, 242 (2012).
[146] Y. Guo, K. Sivalingam, E. F. Valeev, and F. Neese, J. Chem. Phys. **144**, 094111 (2016).
[147] G. Knizia, J. Chem. Theory Comput. **9**, 4834 (2013).
[148] D. Kats, J. Chem. Phys. **145**, 014103 (2016).
[149] J. Nieplocha, B. Palmer, V. Tipparaju, M. Krishnan, H. Trease, and E. Aprà, International Journal of High Performance Computing Applications **20**, 203 (2006).
[150] H.-J. Werner, P. J. Knowles, G. Knizia, F. R. Manby, M. Schütz, *et al.*, "Molpro, version 2015.1, a package of ab initio programs," (2015), see http://www.molpro.net.
[151] T. H. Dunning, Jr., J. Chem. Phys. **90**, 1007 (1989).
[152] R. A. Kendall, T. H. Dunning, and R. J. Harrison, J. Chem. Phys. **96**, 6796 (1992).
[153] T. Dunning, Jr., K. A. Peterson, and A. Wilson, J. Chem. Phys. **114**, 9244 (2001).
[154] F. Weigend, Phys. Chem. Chem. Phys. **4**, 4285 (2002).
[155] F. Weigend, A. Köhn, and C. Hättig, J. Chem. Phys. **116**, 3175 (2002).
[156] H.-J. Werner and P. J. Knowles, J. Chem. Phys. **82**, 5053 (1985).
[157] P. J. Knowles and H.-J. Werner, Chem. Phys. Letters **115**, 259 (1985).
[158] F. Neese, private communication.
[159] B. F. Gherman, W. B. Tolman, and C. J. Cramer, J. Chem. Theory Comput. **27**, 1950 (2006).
[160] C. J. Cramer and W. B. Tolman, Accounts Of Chemical Research **40**, 601 (2007).
[161] R. Polly, H.-J. Werner, F. R. Manby, and P. J. Knowles, Mol. Phys. **102**, 2311 (2004).
[162] C. Köppl and H.-J. Werner, J. Chem. Theory Comput. **12**, 3122 (2016).